ARMY RESEARCH LABORATORY

Computational Flight Design of .50 Caliber Limited Range Training Ammunition

Bernard J. Guidos
Sung K. Chung

ARL-TR-662 January 1995

19950109 093

APPROVED FOR PUBLIC RELEASE; DISTRIBUTION IS UNLIMITED.

NOTICES

Destroy this report when it is no longer needed. DO NOT return it to the originator.

Additional copies of this report may be obtained from the National Technical Information Service, U.S. Department of Commerce, 5285 Port Royal Road, Springfield, VA 22161.

The findings of this report are not to be construed as an official Department of the Army position, unless so designated by other authorized documents.

The use of trade names or manufacturers' names in this report does not constitute endorsement of any commercial product.

REPORT DOCUMENTATION PAGE

Form Approved
OMB No. 0704-0188

Public reporting burden for this collection of information is estimated to average 1 hour per response, including the time for reviewing instructions, searching existing data sources, gathering and maintaining the data needed, and completing and reviewing the collection of information. Send comments regarding this burden estimate or any other aspect of this collection of information, including suggestions for reducing this burden, to Washington Headquarters Services, Directorate for Information Operations and Reports, 1215 Jefferson Davis Highway, Suite 1204, Arlington, VA 22202-4302, and to the Office of Management and Budget, Paperwork Reduction Project(0704-0188), Washington, DC 20503.

1. AGENCY USE ONLY *(Leave blank)*	2. REPORT DATE	3. REPORT TYPE AND DATES COVERED
	Jan 95	Final, February 1993 - April 1994

4. TITLE AND SUBTITLE

Computational Flight Design of .50 Caliber Limited Range Training Ammunition

5. FUNDING NUMBERS

PR: 1L162618AH80

6. AUTHOR(S)

Bernard J. Guidos and Sung K. Chung*

7. PERFORMING ORGANIZATION NAME(S) AND ADDRESS(ES)

U.S. Army Research Laboratory
ATTN: AMSRL-WT-PB
Aberdeen Proving Ground, MD 21005-5066

8. PERFORMING ORGANIZATION REPORT NUMBER

9. SPONSORING/MONITORING AGENCY NAMES(S) AND ADDRESS(ES)

U.S. Army Research Laboratory
ATTN: AMSRL-OP-AP-L
Aberdeen Proving Ground, MD 21005-5066

10.SPONSORING/MONITORING AGENCY REPORT NUMBER

ARL-TR-662

11. SUPPLEMENTARY NOTES

*U.S. Army Armament Research, Development & Engineering Center
Picatinny Arsenal, NJ 07806

12a. DISTRIBUTION/AVAILABILITY STATEMENT

Approved for public release; distribution is unlimited.

12b. DISTRIBUTION CODE

13. ABSTRACT *(Maximum 200 words)*

A computational design study is presented of the aerodynamics and flight behavior of a limited range training round being developed for U.S. Army .50 caliber ammunition. The training round boattail possesses sub-caliber finlets, which impose sufficient spin damping on the projectile to cause it to enter a gyroscopically unstable, high drag flight mode at some distance down range. Aerodynamics coefficients are computed for the training round design and for existing .50 caliber rounds using a parabolized Navier-Stokes viscous flow solver. The aerodynamics coefficients for the existing rounds are compared to range firings. Six-degree-of-freedom trajectory simulations are made to determine the yawing behavior of the training round design, and comparisons are made with Doppler radar test firing results. The present design is evaluated in terms of the flight performance requirement, and design modifications are recommended.

14. SUBJECT TERMS

Computational fluid dynamics, supersonic flow, aerodynamics, trajectories, .50 caliber

15. NUMBER OF PAGES

42

16. PRICE CODE

17. SECURITY CLASSIFICATION OF REPORT	18. SECURITY CLASSIFICATION OF THIS PAGE	19. SECURITY CLASSIFICATION OF ABSTRACT	20. LIMITATION OF ABSTRACT
UNCLASSIFIED	UNCLASSIFIED	UNCLASSIFIED	UL

INTENTIONALLY LEFT BLANK.

TABLE OF CONTENTS

Accesion For

NTIS CRA&I ☒
DTIC TAB ☐
Unannounced ☐
Justification .....

By .....
Distribution /

Availability Codes

Dist	Avail and / or Special
A-1	

INTENTIONALLY LEFT BLANK.

LIST OF FIGURES

1. INTRODUCTION

This report documents a computational aerodynamics and flight design study of a limited range training round being developed for U.S. Army .50 caliber ammunition. The flight requirement for the training round is that it must possess sufficient accuracy for training purposes to a range of 1000 meters, with a maximum range of 2700 meters. The requirement is being satisfied by incorporating a boattail design that features sub-caliber finlets. The finlets impose sufficient roll damping on the projectile to cause it to enter a gyroscopically unstable, high-drag flight mode at some distance down range.

This projectile design will satisfy the need for limited range training ammunition (LRTA) for the existing family of .50 caliber ammunition, which includes (a) API, M8 (Armor Piercing Incendiary), (b) APIT, M20 (API with Tracer), (c) Ball, M33, and (d) M17 (M33 companion tracer round). In addition, the LRTA will likely serve as a design model for its own companion tracer round.

The use of a non-axisymmetric body to impose spin control has been reported (Guidos & Sturek 1987) for small caliber training rounds. That study used unpublished 25-mm design and free-flight range data provided by R.L. McCoy of the former U.S. Army Ballistic Research Laboratory. Twisted, non-axisymmetric boattail designs had previously been examined and later patented by Platou (1974, 1976) as a means of providing spin control.

The focus herein is mainly on the design of the .50 caliber LRTA using simulation techniques. Aerodynamics coefficients for the LRTA and for existing .50 caliber rounds are computed using a three-dimensional parabolized Navier-Stokes (PNS) viscous flow solver. The results for the existing .50 caliber rounds are validated against published range data. Six-degree-of-freedom (6-DOF) trajectory simulations are made to determine the yawing behavior and stable flight range of the LRTA, and comparisons are made with Doppler radar test firing results. The present LRTA design is evaluated in terms of the performance requirement, and design modifications are recommended.

2. CONFIGURATIONS AND FLIGHT CONDITIONS

Three existing U.S. Army .50 caliber projectiles are shown in Figure 1. They are identified as (a) API, M8, (b) APIT, M20, and (c) Ball, M33. McCoy (1990) has published background information about these configurations as well as aerodynamics results from previous free flight range tests. The range results for the API, M8 and the Ball, M33 are used in this study. For brevity, the two projectiles are subsequently referred to as M8 and M33. The external

geometries of these rounds differ only in minor surface details such as rolled versus machined cannelures. Figure 2 is a schematic of the single external geometry used to computationally model both the M8 and M33 projectiles. The computational geometry does not include any of the surface protuberances found on the actual rounds.

The physical characteristics of the M33 projectile are listed in Table 1. The M8 and M33 projectiles have centers of gravity (CG) locations that differ by only about 0.2% of their total lengths, so differences in moment coefficients attributable to this CG difference are negligible.

Table 1. Projectile Physical Characteristics

	M33	LRTA
Reference Diameter (mm)	12.95	12.95
Length (calibers)	4.46	5.21
Mass (g)	42.0	43.7
CG (calibers from base)	1.78	2.70
I_{xx} (g·cm^2)	7.85	8.49
I_{yy} (g·cm^2)	74.5	101.8

The .50 caliber LRTA design is shown schematically in Figure 3. For simplicity, the nose section geometry is assumed to be identical to the M33, although the actual blueprints (not presented here) show subtle differences between the two configurations. The physical characteristics used to model the LRTA design are included in Table 1. The LRTA boattail design consists of a short 7° axisymmetric section followed by a non-axisymmetric section of length slightly greater than one caliber. This non-axisymmetric boattail section is formed by engraving the cylindrical section with a mill cutter to form four sub-caliber finlets.

Figure 4 shows the computational surface model of the LRTA configuration. For clarity, most of the computational surface grid points are omitted from the plot. The LRTA computational boattail model is a simplified version of the actual design in that surface discontinuities are somewhat smoothed. This is a characteristic of the fin geometry model (Rai, Chaussee, & Rizk 1983; Weinacht, Guidos, Sturek & Hodes 1986), used here with minor modifications. The cross section of the computational boattail geometry consists of an axisymmetric body which is smoothly coupled with spherically tipped fins. In contrast, the cross section of the actual boattail section (refer to Figure 3) is more aptly described as a square body coupled with square-tipped fins. The following approach was used to provide an appropriate computational boattail geometry model for the LRTA.

The actual square boattail body is modeled using an axisymmetric cross section whose

radius r_{bt} varies smoothly in accordance with the relation

$$r_{bt} = r_{min} + r_{fac}(r_{ref} - r_{min}) \tag{1}$$

in which r_{ref} is one-half the reference diameter d, and r_{min} is the minimum radius of the boattail cross section. The variable r_{fac} is a factor whose value decreases continuously and monotonically from one to zero. This factor is defined using the 5th order polynomial expression

$$r_{fac} = 10\left(\frac{x_{end} - x}{x_{end} - x_{beg}}\right)^3 - 15\left(\frac{x_{end} - x}{x_{end} - x_{beg}}\right)^4 + 6\left(\frac{x_{end} - x}{x_{end} - x_{beg}}\right)^5 \quad \text{for} \quad x_{beg} < x < x_{end} \tag{2}$$

in which x is the axial location of the cross section of interest (measured from the spherical nosetip vertex), x_{beg} is the axial location of the cylinder-boattail juncture, and x_{end} is the axial location where the boattail radius reaches its minimum value. For $x > x_{end}$, r_{bt} is equal to r_{min}, i.e., the cross section remains unchanged.

Two different LRTA computational boattail geometry configurations were generated by assigning two sets of boattail geometry parameters, and these values are shown in Table 2. The two configurations are intended to form a geometric bound for the planform area of the finlets of the actual design. In turn, the two configurations are expected to form a corresponding bound on the aerodynamic coefficients for the LRTA. The essential difference between the two configurations is that Configuration #2 has more fin planform area than Configuration #1.

Table 2. LRTA Boattail Computational Geometry Parameters (in Calibers)

	x_{beg}	x_{end}	r_{min}
Configuration #1	3.75	4.47	0.37
Configuration #2	3.75	4.63	0.26

The service launch velocity for all rounds is taken to be Mach 2.6. Atmospheric sea level free stream conditions are assumed for all computations. Computational results are presented for free stream Mach numbers 1.5, 1.96, and 2.6. The Reynolds numbers for these velocities are taken as 34.0 million, 44.5 million, and 59.0 million, respectively, based on a length of 1 meter. The wall temperature is specified as 294 K, and the flow is assumed to be fully turbulent.

Angles of attack are prescribed as 0° or 2°. The roll orientation for the non-axisymmetric configurations is such that two finlets are aligned with the pitch plane. The magnitudes of the nondimensional spinning and coning rates are prescribed in the range from 0.0 to 0.01 for various computational runs. The direction of positive spinning and positive coning is

clockwise as viewed from the projectile base. The force, moment, and spin conventions follow those put forth by Murphy (1963).

3. PARABOLIZED NAVIER-STOKES CFD TECHNIQUE

The PNS technique has been adapted and extensively used within the Weapons Technology Directorate of the U.S. Army Research Laboratory (ARL) and is a powerful computational fluid dynamics (CFD) research tool for predicting supersonic and hypersonic projectile aerodynamics. The PNS technique is a space-marching (as opposed to a time-marching) technique; that is, one numerical integration sweep is made from the nosetip of the projectile to the base to obtain a single steady state solution. Each solution for the M33 projectile at angle of attack used about 5 minutes of processing time on a Cray X-MP computer. Each solution for the LRTA configuration used about 15 minutes.

The PNS technology was first applied to U.S. Army projectiles to compute static pitch-plane and Magnus coefficients for spinning and non-spinning shell and for wind tunnel models at various angles of attack (Sturek & Schiff 1981; Schiff & Sturek 1981). Similar applications were made to shell at moderate angle of attack and to finned KE projectiles (Weinacht, Guidos, Kayser, Sturek 1985; Weinacht, Guidos, Sturek, Hodes 1986). The technique was modified to compute roll characteristics of finned KE projectiles with exact fin geometry using a rotating coordinate frame (Weinacht & Sturek 1988). Further modifications were added to compute the pitch damping of axisymmetric (Weinacht, Sturek, & Schiff 1991) and finned (Weinacht & Sturek 1990) projectiles using a coning coordinate frame.

The PNS technique introduced by Schiff and Steger (1979) is a three-dimensional, finite difference, viscous flow solution procedure for attached supersonic and hypersonic flow fields. The PNS technique spatially integrates the dimensionless, transformed, steady, thin layer, mass-averaged Navier-Stokes equations in strong conservation law form. The governing equations represent steady state conservation of mass, momentum, and energy in transformed coordinates for large Reynolds number flows. The Cartesian form of the equations is

$$\frac{\partial \hat{E}_s}{\partial \xi} + \frac{\partial \hat{F}}{\partial \eta} + \frac{\partial \hat{G}}{\partial \zeta} = \hat{R}e^{-1}\frac{\partial \hat{S}}{\partial \zeta} \tag{3}$$

These equations were recast in cylindrical coordinates and applied by Rai and Chaussee (1983). The major advantage is that the cylindrical coordinate formulation requires only three circumferential grid planes for axisymmetric flow cases within the framework of the bilateral symmetry that is imposed. The cylindrical form of the governing equations is

$$\frac{\partial \hat{E}_s}{\partial \xi} + \frac{\partial \hat{F}}{\partial \eta} + \frac{\partial \hat{G}}{\partial \zeta} + \hat{H}_c = \hat{Re}^{-1}(\frac{\partial \hat{S}}{\partial \zeta} + \hat{S}_c) \tag{4}$$

The vectors $\hat{E}_s$, $\hat{F}$, and $\hat{G}$ contain the transformed inviscid fluxes. $\hat{E}_s$ is a modified flux vector resulting from the subsonic sublayer approximation (Schiff & Steger 1979). The vector $\hat{S}$ is the transformed vector of viscous terms that results from the thin layer approximation. The vectors $\hat{H}_c$ and $\hat{S}_c$ contain inviscid and viscous source terms, respectively, resulting from the cylindrical coordinate formulation. The components of the vectors for the Cartesian formulation are given in many sources, including Schiff & Steger. The components of all the vectors for the cylindrical formulation are given by Weinacht and Sturek (1990). The three transformed coordinates are $\xi = \xi(x)$, the axial (marching); $\eta = \eta(x, y, z)$, the circumferential coordinate; and $\zeta = \zeta(x, y, z)$, the radial coordinate. The transposed vector of dependent variables is defined as

$$\bar{Q} = [\rho, \rho u, \rho v, \rho w, \varepsilon] \tag{5}$$

in which the density is ρ; the axial, circumferential, and radial velocity components are u, v, and w, respectively. The total energy per unit volume is ε.

The solution is obtained at each grid point using the approximately factored, implicit, delta form, finite difference algorithm of Beam and Warming (1978). Second order central differencing is used in the circumferential and radial directions, and first order one-sided differencing is used in the marching direction. The solution is advanced downstream by numerically integrating in the main flow direction. Each marching step requires a series of block tridiagonal matrix inversions (sweeps) in the circumferential and radial directions. Fourth order explicit smoothing terms are added to suppress high frequency oscillations. Second order implicit smoothing terms are added to maintain numerical stability in regions of large pressure gradients (such as fin leading edges). Initial conditions for marching are generated using the PNS method in step-back mode (Sturek & Schiff 1981), which assumes conical flow conditions near the nosetip and iteratively refines the solution to satisfy this assumption.

Perfect gas behavior is assumed. Turbulence is accounted for using the two-layer, algebraic eddy viscosity model of Baldwin and Lomax (1978). In that model, the inner wall layer eddy viscosity is computed using a conventional Prandtl mixing length with Van Driest damping. The outer, or wake, layer eddy viscosity is based upon an evaluation of the maximum moment of vorticity and its distance from the wall. The calculation of the eddy viscosity is lagged by one marching step.

The outer boundary, which consists of the bow shock, is shock fitted using the implicit

procedure reported by Rai and Chaussee (1983). The no-slip condition is enforced at the body surface and the pressure is held constant across the subsonic portion of the boundary layer (i.e., the subsonic sublayer approximation). The energy is defined from the pressure using the perfect gas law. The wall temperature is specified, and the density is determined from the temperature and pressure.

4. RESULTS

4.1 Aerodynamic Coefficients for M8 and M33. Aerodynamics computations were performed for the M8 and M33 projectiles and the aerodynamics coefficients were compared to free flight range data published by McCoy (1990). The experimentally obtained aerodynamic coefficients were produced from standard yaw-drag fits of the equations of free flight motion from Murphy (1963). Since the CFD results were generated at small angles of attack, aerodynamic coefficients from range firings with average angles of attack greater than 5° were excluded from the comparisons to avoid introducing large angle-of-attack nonlinearities into the analysis.

The pitch-plane range data are published as the lift force coefficient, C_{L_α}, and the computational pitch-plane results are in the form of normal force coefficient, C_{N_α}. The lift force coefficient was converted here into the normal force coefficient by employing the measured drag coefficient, C_D, and the trigonometric relationship

$$C_N = C_L \cos\alpha + C_D \sin\alpha \tag{6}$$

in which C_N and C_L are normal and lift force coefficients, respectively, at a specific angle of attack. The relationship is simplified by assuming small angle of attack into

$$C_{N_\alpha} = C_{L_\alpha} + C_D \tag{7}$$

In Figure 5, the comparison of pitching moment coefficient, C_{M_α}, for the M8 and M33 projectiles is shown. The computed value at Mach 2.6 is within the scatter of the range data, which is about 15%. The value at Mach 1.5 is within about 5% of the data; the value at Mach 1.95 is within 10% of the data. Figure 6 shows the comparison of normal force center of pressure, CP_N. The computed values at Mach 2.6 and Mach 1.96 are within the scatter of the data. The computed value at Mach 1.5 is about 0.15 calibers forward of the measured value. Figure 7 shows the comparison of normal force coefficient, C_{N_α}. The computed values are within the scatter of the data or within about 5% except at Mach 1.5, which is off by about 15%.

Figure 8 shows the comparison of Magnus moment coefficient, $C_{M_{p\alpha}}$. Most of the range

data indicate that the M8 has a positive Magnus moment below Mach 1.5, while the M33 has a negative Magnus moment. The computed values indicate a positive Magnus moment at all three Mach numbers. The computed value at Mach 2.6 is within the scatter of the data. At Mach 1.96 and Mach 1.5, $C_{M_{p\alpha}}$ is overpredicted by amounts which are about the same as the scatter of the data. The range values of $C_{M_{p\alpha}}$ below M=1.5 vary widely, indicating the degree of difficulty in obtaining repeatable Magnus measurements for the M8 and M33 projectiles. Figures 9 and 10 show the computed values of Magnus force coefficient, $C_{N_{p\alpha}}$, and Magnus force center of pressure, CP_M. These coefficients were not obtained from the range firings.

Figure 11 shows the computed and measured values of pitch damping moment coefficient, $C_{M_q} + C_{M_{\dot{\alpha}}}$. At Mach 2.6, the computed value is within the scatter of the range data, while at Mach 1.96 and Mach 1.5, the computed values agree within about 10% of the data.

Figure 12 shows the computed values of roll damping coefficient, C_{l_p}. The roll damping coefficient was not obtained in the range firings since the configurations were not fitted with roll pins. It is noted that the roll damping is held constant with respect to angle of attack in the 6-DOF simulations to be presented.

Figure 13 shows the computed and measured values of zero-yaw drag coefficient, C_{D_o}. Three sets of predicted values of C_{D_o} are shown. The first is the PNS result. The second includes a nosetip contribution obtained by integrating a modified Newtonian pressure distribution (Anderson 1990). The third includes a base drag contribution as predicted by the semi-empirical 'McDrag' code (McCoy 1981). The range results are bound by the second and third sets of predicted drag values.

4.2 Aerodynamic Coefficients for LRTA. Aerodynamics coefficients for the two LRTA configurations were computed using the same velocities and free stream conditions as the M8 and M33 configurations. The LRTA results at Mach 1.5 contain unwanted numerical oscillations over the final 1/2 caliber or so, and efforts to dampen the oscillations were unsuccessful. These oscillations (which are shown in a subsequent figure) are not unexpected since Mach 1.5 is an extremely low velocity at which to apply the PNS technique. The results are included here for completeness and for future reference.

Figures 14, 15, and 16 show C_{N_α} as a function of x/d for Configurations #1 and #2 at the three Mach numbers of interest. The computed results are shown for the current design length of 5.2 calibers and for lengths extending approximately two calibers beyond. At the current design length, C_{N_α} of Configuration #2 is about 10% larger than that of Configuration #1. Figures 17, 18, and 19 show CP_N as a function of x/d at the three Mach

numbers. At the current design length, CP_N of Configuration #2 is about 1/4 caliber farther rearward than that of Configuration #1. The decrease of C_{N_α} and CP_N as boattail length increases is a behavior that has already been observed for conical boattail configurations in supersonic flow (Weinacht, et al 1985). C_{N_α}, CP_N, and CG are input into the 6-DOF trajectory simulation code and determine C_{m_α}, which influences the gyroscopic stability of the projectile.

Figures 20, 21, and 22 show C_{l_p} as a function of x/d at the three Mach numbers. The computational results show the magnitude of C_{l_p} for the LRTA configurations to be about 5 times greater than the M8 and M33 configurations. At the current design length, C_{l_p} of Configuration #2 is about 30% greater than that of Configuration #1, demonstrating the large sensitivity of C_{l_p} to fin planform area. The numerical oscillations previously mentioned at Mach 1.5 are apparent in Figure 22. In addition, the figures show C_{l_p} to decrease with respect to x/d over a small portion of the boattail at all three Mach numbers before increasing again. This computed decrease in C_{l_p} with respect to x/d is an unexpected result. The phenomenon was investigated by computing the flow field for Configuration #1 but with two opposing fins removed. Figure 23 shows C_{l_p} with respect to x/d for the 2-fin and 4-fin configurations at Mach 1.96. The 2-fin design does not show a decrease in roll damping with respect to x/d. It may be concluded that computed decreases in C_{l_p} with respect to x/d are attributable to the computed interaction of adjacent fins subjected to the expansion and recompression of the flow over the boattail region.

Figure 24 shows the computed $C_{M_q} + C_{M_{\dot{\alpha}}}$ of the LRTA Configurations #1 and #2 at the three Mach numbers of interest. The magnitude of this coefficient is about 15% greater for Configuration #2 than for Configuration #1 and is approximately twice that of the M8 and M33 projectiles.

Figures 25 and 26 show the computed C_{D_O} of the LRTA Configurations #1 and #2, respectively, at the three Mach numbers of interest. The predictions consist of the PNS result, a modified Newtonian nosetip contribution, and a base drag estimate. The base drag estimate was formed by determining and integrating an average base pressure over the base of the two configurations. The average base pressure of the two LRTA configurations was taken to be the same as the estimated M33 base pressure at each Mach number. Using this approach, the computed drag of both LRTA configurations is predicted to be less than that of the M8 and M33 projectiles.

The Magnus force and moment coefficients are the only aerodynamic coefficients not presented for the LRTA but required for the 6-DOF simulation. Direct computation of the Magnus coefficients for non-axisymmetric bodies has yet to be accomplished using CFD

technology. For typical non-axisymmetric projectile configurations, such as finned kinetic penetrators, the Magnus coefficients are not critical because the spin rates are comparatively low. The .50 caliber LRTA, however, uses spin rates large enough to require consideration of Magnus effects. A large Magnus moment could conceivably dominate the overall stability characteristics of the LRTA, causing dynamic instability even though the round is gyroscopically stable.

The Magnus force and moment for an axisymmetric body is predominantly comprised of a pressure contribution that arises from asymmetric boundary layer interaction with the inviscid flow field (Sturek & Schiff 1981). The presence of fins gives rise to a separate contribution in which the force acts in the opposite direction (Platou 1963). In the present analysis, the computed Magnus coefficients of the M33 projectile are used in the LRTA 6-DOF trajectory simulations. It is assumed that the Magnus contribution attributable to the fins is zero. The Magnus coefficients of the LRTA could probably be obtained from indoor range firings, and a computational capability to predict Magnus moment coefficient for a non-axisymmetric projectile would be valuable in a study such as this.

4.3 6-DOF Trajectory Simulations. Using the predicted aerodynamic coefficients, 6-DOF simulations were performed using the code whose development is described by Fiorellini and Grau (1992). The launch velocity is taken as Mach 2.6. The quadrant elevation is 30°. The initial roll rate is 14627.0 rad/s, corresponding to a rifled bore with a twist of one revolution per 30 calibers of travel. The initial yaw angle is set to zero, and initial yawing rate is set to 3 rad/s. Aerodynamic coefficients are supplied at the three Mach numbers discussed above, with linear interpolation between Mach numbers and linear extrapolation below Mach 1.5.

Figure 27 shows the computed Mach number versus range for both LRTA configurations. Both configurations exhibit virtually the same Mach number behavior over the first 500 meters of flight. The simulation for Configuration #1 reaches 1000 meters range, where the Mach number is about 1.5.

Figure 28 shows the computed gyroscopic stability factor, S_g (Murphy 1963), versus range for both LRTA configurations. The gyroscopic stability factor is proportional to the square of the roll rate and inversely proportional to the pitching moment coefficient. Following Murphy's discussion, a projectile is gyroscopically stable if S_g is greater than unity. Configuration #1 is launched with a gyroscopic stability factor of about 1.6 and decreases to a value of 1.0 at a range of about 750 meters. Configuration #2 is launched with a gyroscopic stability factor of about 2.0 and decreases to a value of 1.0 at a range of about 450 meters.

The in-flight decrease of S_g for both configurations is primarily attributable to a reduction in the nondimensional spin rate, pd/V_∞, shown in Figure 29.

Figure 30 shows the computed angle of attack versus range for both LRTA configurations. Both configurations are computed to damp throughout the early portion of flight. Configuration #1 experiences rapid yaw growth at a range of about 875 meters, about 125 meters down range from where it becomes gyroscopically unstable. Configuration #2 experiences rapid yaw growth at a range of about 525 meters, about 75 meters downrange from where it becomes gyroscopically unstable. Therefore, the LRTA is predicted to damp throughout the early portion of its flight and experience rapid yaw growth above 1° at a range between 525 and 875 meters. Results beyond this portion of the flight were not obtainable since the aerodynamic coefficients are applicable only for small angles of attack.

4.4 Doppler Radar Measurements & Discussion. During February 1994, Doppler radar tests were conducted by the U.S. Army Combat Systems Test Activity at Aberdeen Proving Ground, Maryland for the M33 and LRTA configurations. Doppler effect radar tracking system model W1000 from Weibel Inc. of Denmark was used to obtain the in-flight total drag coefficient, C_D. The launch velocity is about Mach 2.6 and the quadrant elevation is 25°. Usable data were obtained from approximately 10 rounds each for the M33 and LRTA configurations.

Figure 31 shows a representative result of measured in-flight total drag for the M33 and LRTA. The LRTA experiences a rapid increase in C_D at a range of about 1000 meters. It is assumed that this increase in drag, to values an order of magnitude larger than the launch values, is caused by a rapid increase in yaw brought about by the onset of gyroscopic instability.

An important observation of Figure 31 is that the measured LRTA and M33 drag coefficients are about the same at launch. (These data and the actual mean data show the LRTA to have slightly greater drag than the M33 at launch.) The CFD predictions (see Figures 13, 23, and 24) show the opposite trend for zero-yaw drag, i.e., that the M33 has a higher zero-yaw drag than the LRTA. Since the yaw drag is included in the Doppler measurement, a direct comparison of drag cannot be made between the measured and predicted drag values. However, if the measured and predicted drag trends are both correct, then it may be concluded that the LRTA experiences larger initial launch disturbances than the M33. These disturbances would result in larger initial yaw levels and increased total drag at launch.

Figure 31 also shows that the LRTA drag coefficient grows significantly even before it reaches 1000 meters range. The growth is noticeably larger than that of the M33, suggesting

that the LRTA is experiencing yaw drag effects not predicted in the 6-DOF simulation. Two possible explanations are as follows: (1) the yaw levels in the actual round are not damping as fast as those in the 6-DOF simulation and (2) the yaw levels are actually growing (i.e., the round is dynamically unstable).

A possible source of dynamic instability in the LRTA is the Magnus moment. As previously mentioned, direct prediction of the Magnus moment for the LRTA was not performed. Instead, the predicted Magnus moment for the M33 was used in the 6-DOF simulation. The sensitivity of the dynamic stability to Magnus effects was briefly studied here. The projectile is dynamically stable if the following relationship between the dynamic stability factor, S_d, and the gyroscopic stability factor is satisfied (Murphy 1963):

$$S_d(2 - S_d) > \frac{1}{S_g} \tag{8}$$

The dynamic stability factor depends primarily on the Magnus moment and pitch damping moment coefficients. The sensitivity of the dynamic stability to the Magnus moment coefficient was studied by examining a stability coefficient, S_d^*, which reflects the relationship between the two stability factors. The stability coefficient is defined here as

$$S_d^* = S_d(2 - S_d) - \frac{1}{S_g} \tag{9}$$

where the projectile is dynamically stable if S_d^* is positive, in which case, the maximum yaw is expected to decrease with respect to range.

The stability coefficient was calculated for a parametric variation of Magnus moment coefficient at ranges of 0 and 560 meters (corresponding to in-flight Mach numbers 2.6 and 1.96, respectively). The in-flight velocities, spin rates, and aerodynamic coefficients from the 6-DOF simulation (Configuration #1) were used. Figure 32 shows that the Magnus values used in the 6-DOF simulation provide dynamic stability. However, the figure also shows that possible fin Magnus moment contributions (which will be negative in sign) of equal magnitude to the Magnus moment values used in the 6-DOF simulation could cause dynamic instability.

It cannot be conclusively determined from the radar tests alone whether the current LRTA design possesses sufficient accuracy for training purposes at a range of 1000 meters. However, it is noted that recent dispersion test results (not included here) show that (1) the M33 forms a tighter impact group than the LRTA (2) some of the LRTA projectiles show considerable yaw at 1000 meters, and (3) the mean point of impact is within 1 mil.

The aerodynamic coefficients presented here provide sufficient guidance for possible design modifications. One recommended modification is shortening the boattail, which would

reduce the roll damping and increase the stable flight range of the projectile. A shorter boattail would also reduce the fin Magnus effect and would likely reduce initial launch disturbances, resulting in improved dispersion characteristics over the present design.

Finally, it is noted that the Doppler radar results showed the maximum range of the LRTA to be about 1800 meters, well within the 2700 meter maximum range requirement. For comparison, it is noted that the radar showed the maximum range of the M33 to be about 6000 meters.

5. CONCLUSION

A computational aerodynamics and flight design study for .50 caliber limited range training ammunition (LRTA) has been presented. The LRTA possesses sub-caliber finlets that impose sufficient roll damping on the projectile to cause it to enter a gyroscopically unstable, high drag flight mode at some distance down range. A three-dimensional parabolized Navier-Stokes (PNS) viscous flow solver was applied to compute the aerodynamic coefficients for the LRTA and for existing .50 caliber M8 and M33 projectiles. The PNS results were validated against published range data. The computed aerodynamic coefficients were used in six-degree-of-freedom (6-DOF) trajectory simulations to determine the yawing behavior and stable flight range of the LRTA. Doppler radar test firing measurements for the LRTA were presented.

The PNS predictions for the M8 and M33 configurations agree with the range data mostly within the experimental scatter. PNS predictions for the LRTA were made for two computational geometries expected to bound the aerodynamic behavior of the actual LRTA, which consists of a relatively complex and discontinuous surface geometry. The roll damping coefficient of the two configurations is predicted to differ by about 30%, demonstrating the large sensitivity of this coefficient to small changes in fin planform area for the LRTA.

The 6-DOF trajectory simulations show significant differences in the stable flight range for the two computational configurations. Configuration #1 is predicted to maintain low angle-of-attack flight to a range of about 875 meters, while Configuration #2 is predicted to maintain low angle-of-attack flight to a range of about 525 meters. The Doppler radar measurements show the actual LRTA to maintain low angle-of-attack flight to a range of about 1000 meters. The Doppler radar measurements also show evidence that the LRTA experiences larger yaw levels than the M33, as well as possible dynamic instability because of Magnus effects in the first 1000 meters of flight. The measurements show the maximum range of the current LRTA design to be about 1800 meters, well within the requirement of

2700 meters.

The aerodynamic coefficients presented here provide sufficient guidance for possible design modifications. One recommended modification is a shortening of the boattail, which would reduce the roll damping and extend the stable flight range of the projectile. A shorter boattail would also reduce the fin Magnus effect and would likely reduce initial launch disturbances, resulting in improved dispersion characteristics over the present design.

The use of sub-caliber finlets for .50 caliber limited range training ammunition appears to be a viable concept. The present .50 caliber LRTA design is close to satisfying the flight requirements for this mission. Such a non-axisymmetric boattail concept is also being pursued for application to 5.56-mm limited range training ammunition. Overall, the flight design analysis presented in this study demonstrates how state-of-the-art CFD technology and experimental development programs together form a powerful projectile design capability.

INTENTIONALLY LEFT BLANK.

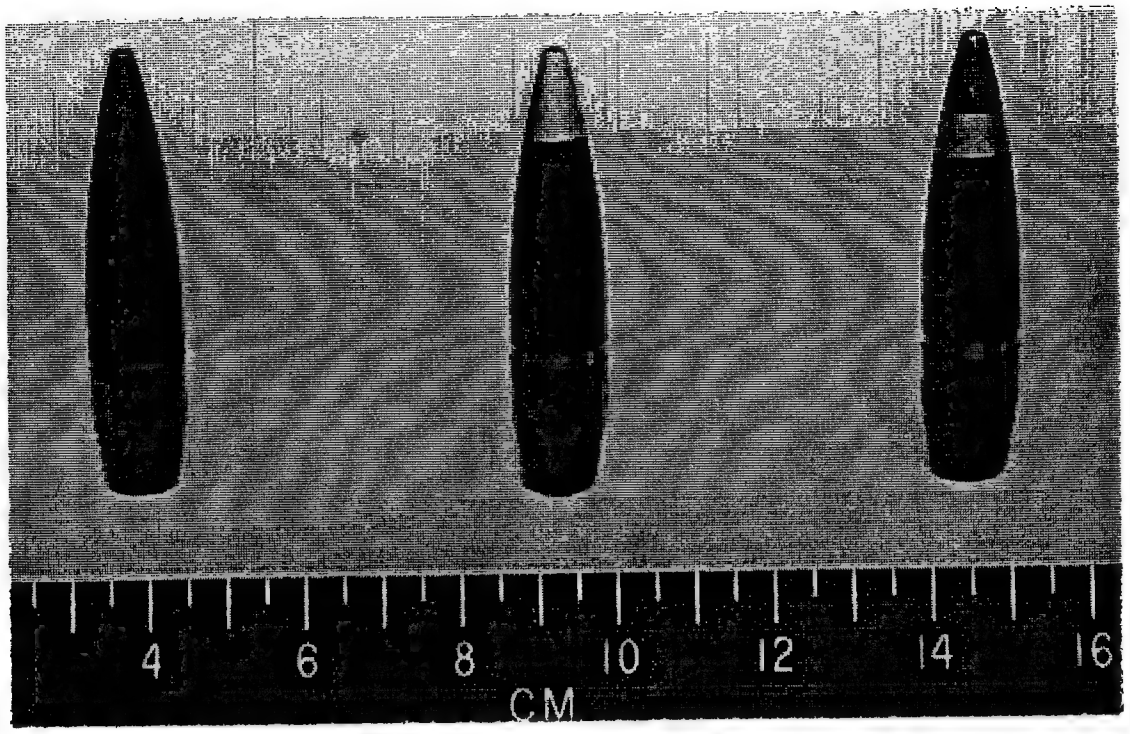

Figure 1. Photograph of (a) API, M8, (b) APIT, M20, and (c) Ball, M33 .50 Caliber Projectiles

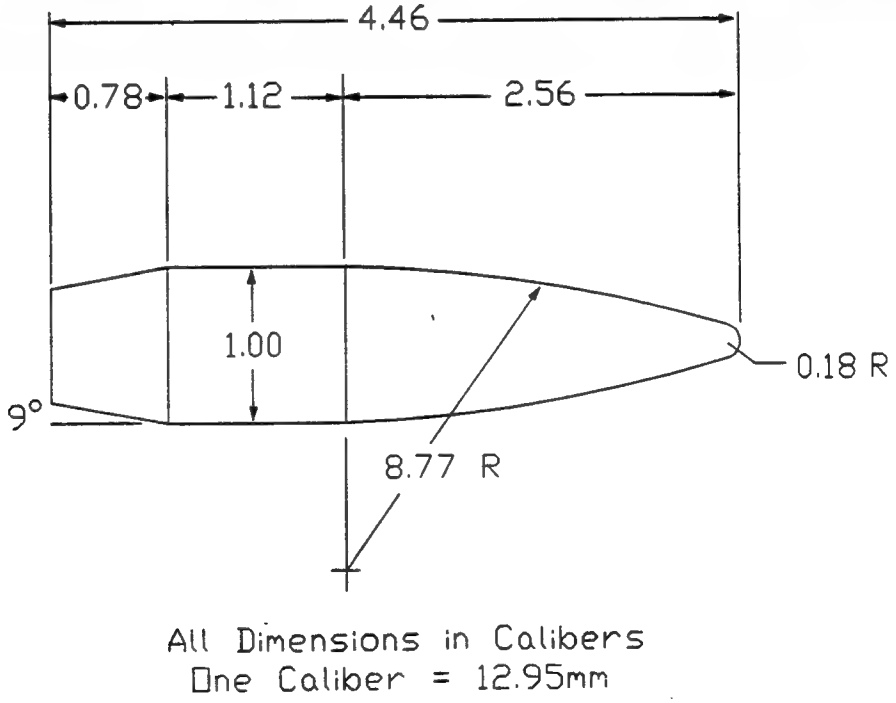

Figure 2. Schematic of .50 Caliber Ball, M33 Projectile

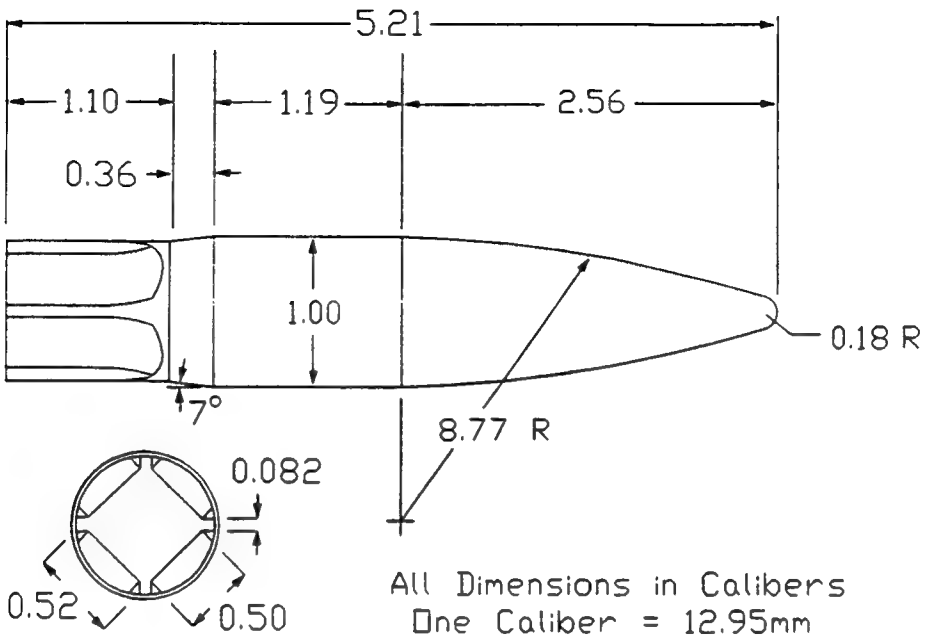

Figure 3. Schematic of .50 Caliber Limited Range Training Ammunition (LRTA) Design

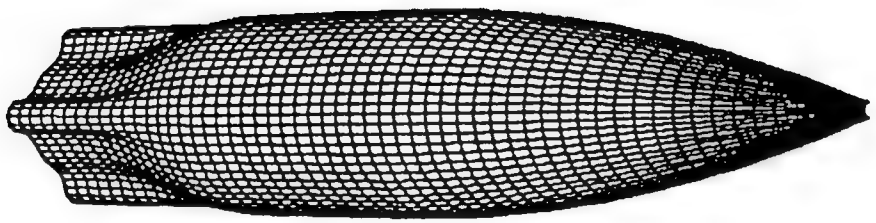

Figure 4. Computational Surface Geometry Model of LRTA

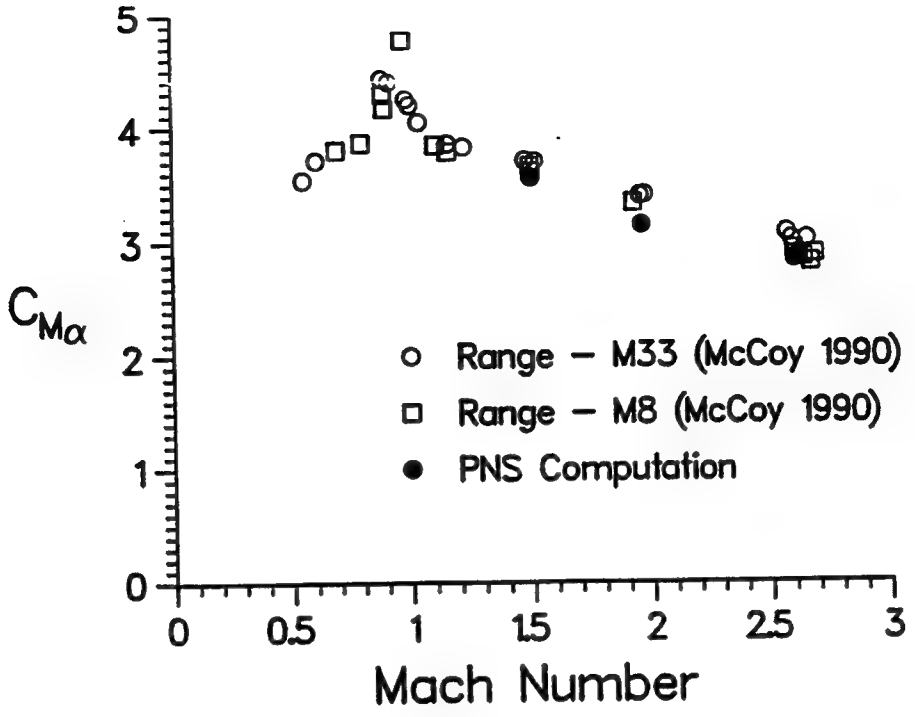

Figure 5. Computed and Measured Pitching Moment Coefficient Versus Mach Number, M8 and M33 Projectiles

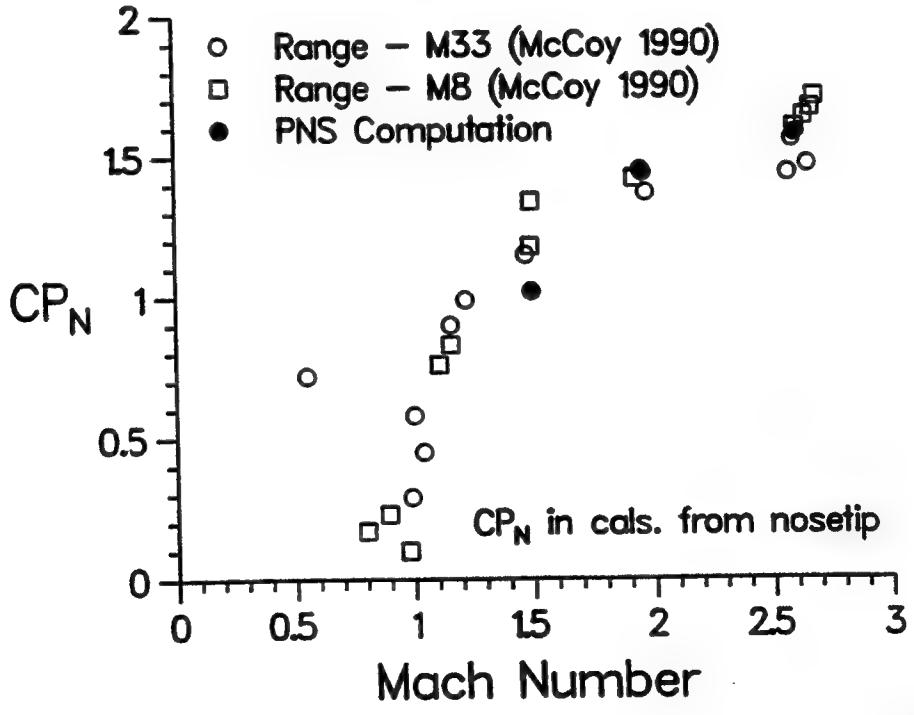

Figure 6. Computed and Measured Normal Force Center of Pressure Versus Mach Number, M8 and M33 Projectiles

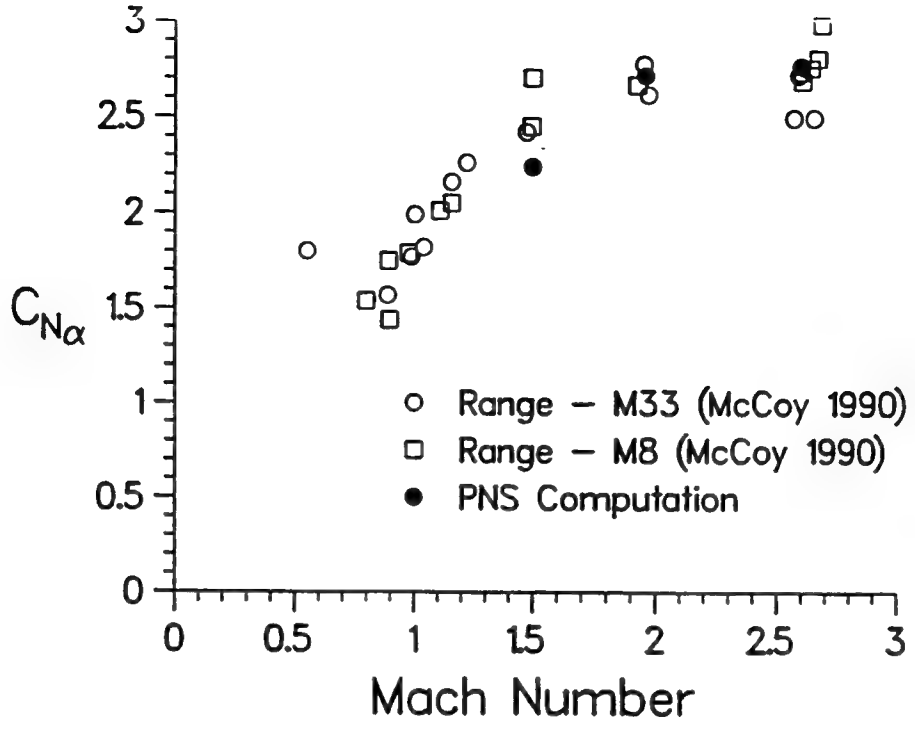

Figure 7. Computed and Measured Normal Force Coefficient Versus Mach Number, M8 and M33 Projectiles

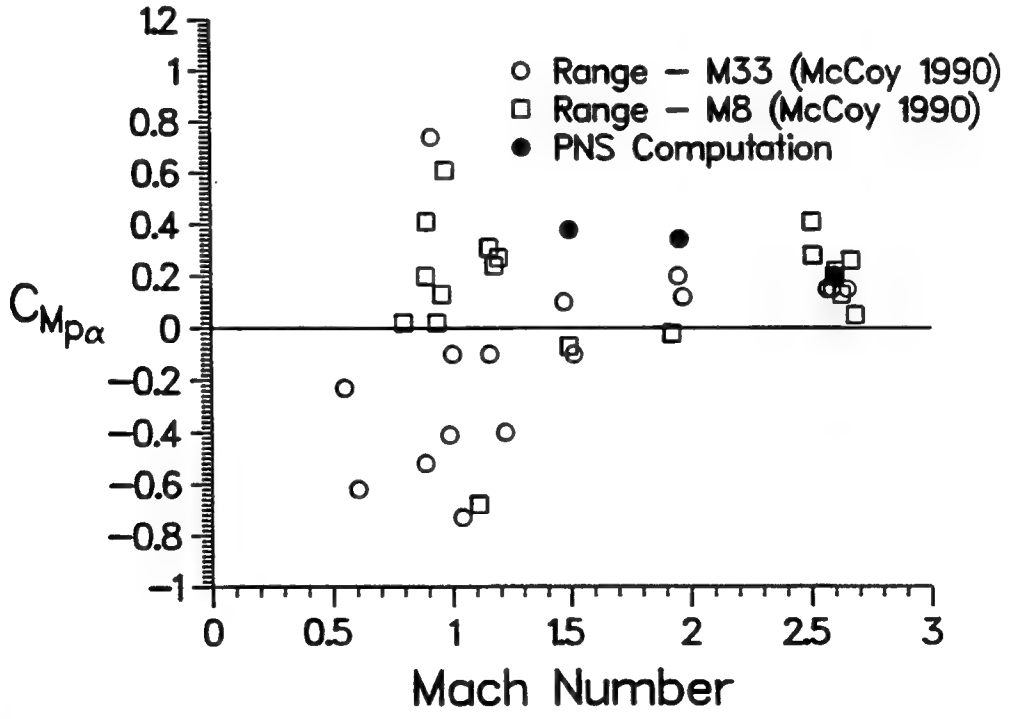

Figure 8. Computed and Measured Magnus Moment Coefficient Versus Mach Number, M8 and M33 Projectiles

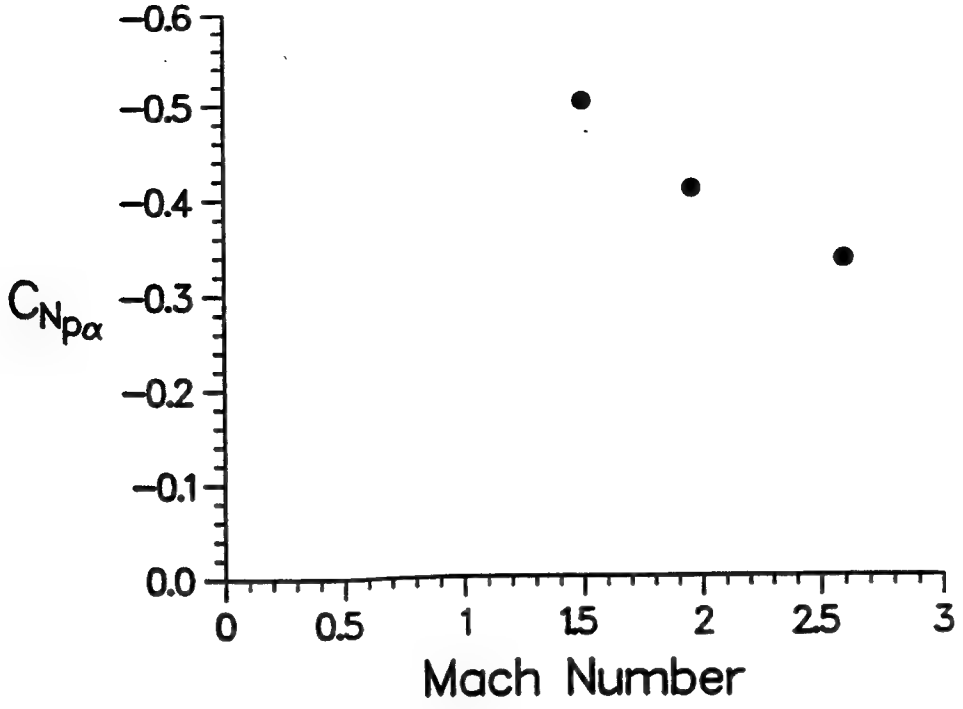

Figure 9. Computed Magnus Force Coefficient Versus Mach Number, M8 and M33 Projectiles

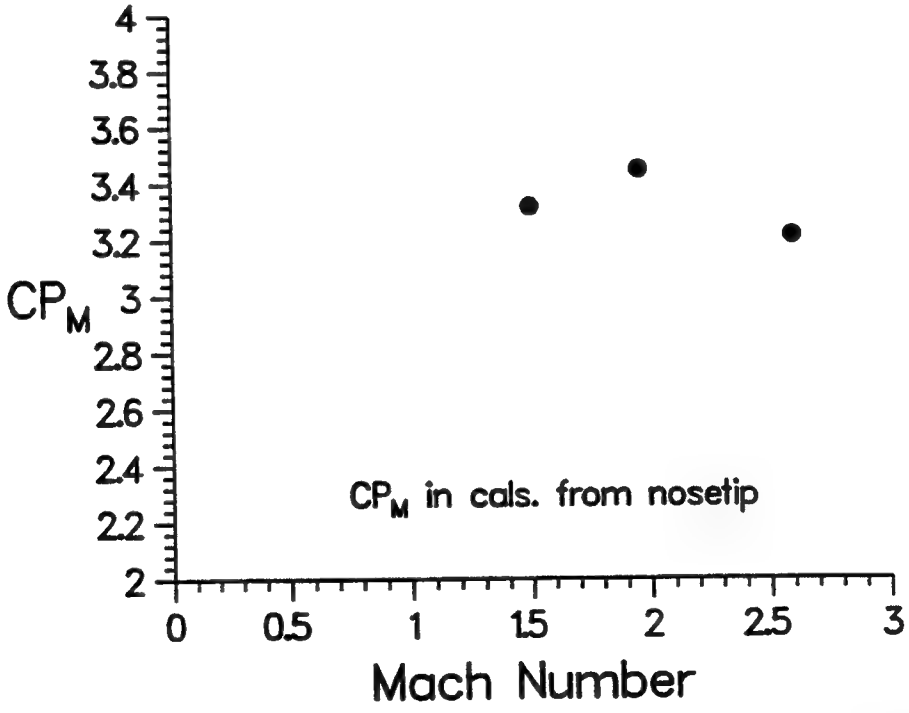

Figure 10. Computed Magnus Force Center of Pressure Versus Mach Number, M8 and M33 Projectiles

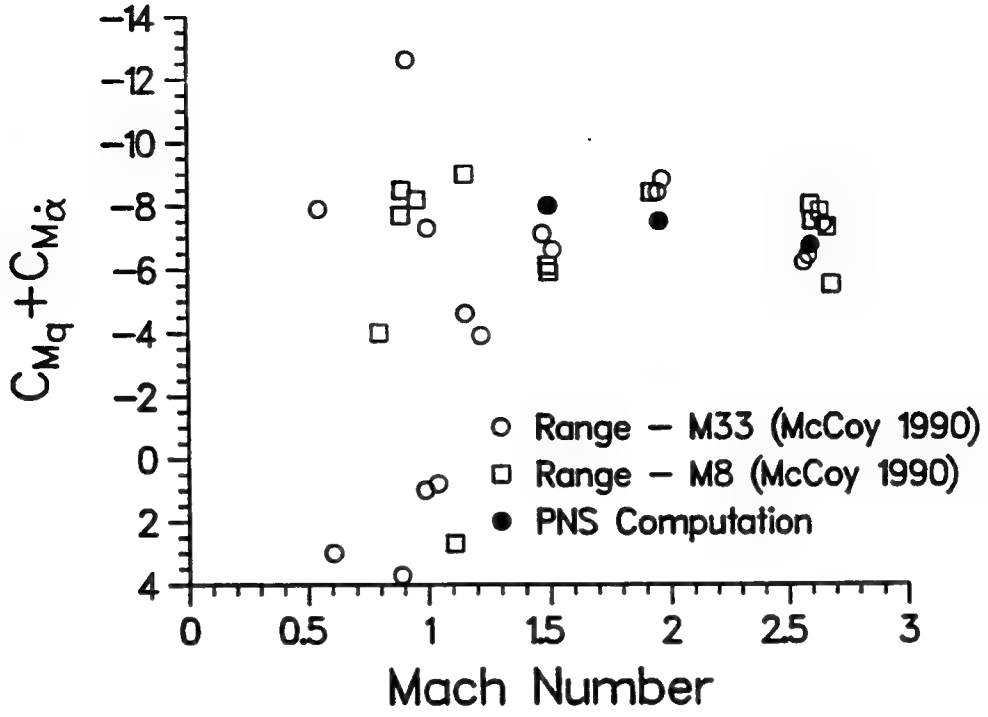

Figure 11. Computed and Measured Pitch Damping Moment Coefficient Versus Mach Number, M8 and M33 Projectiles

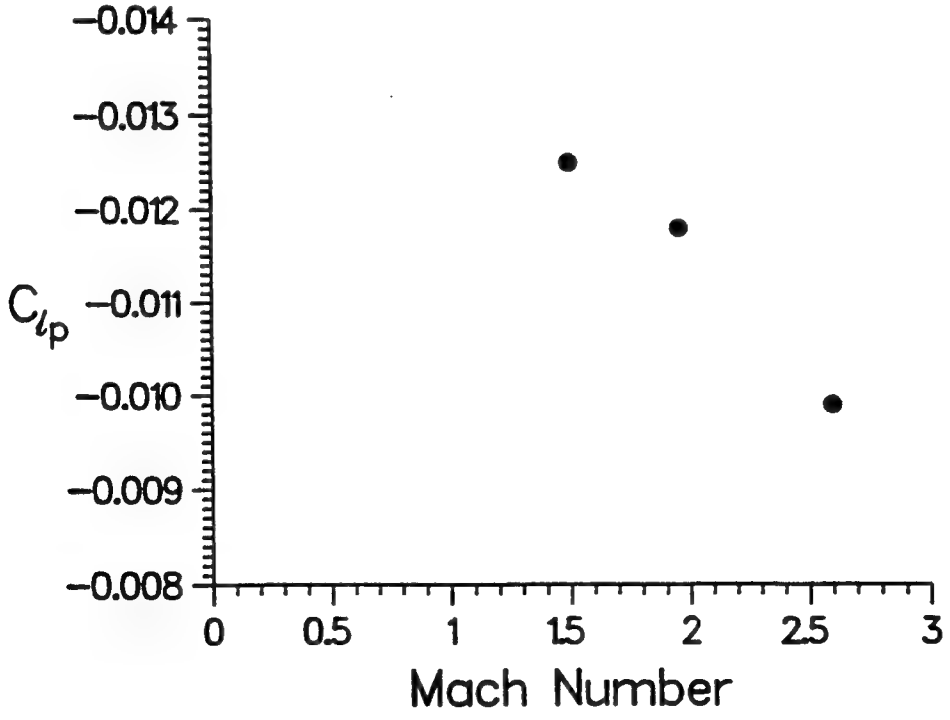

Figure 12. Computed Roll Damping Coefficient Versus Mach Number, M8 and M33 Projectiles

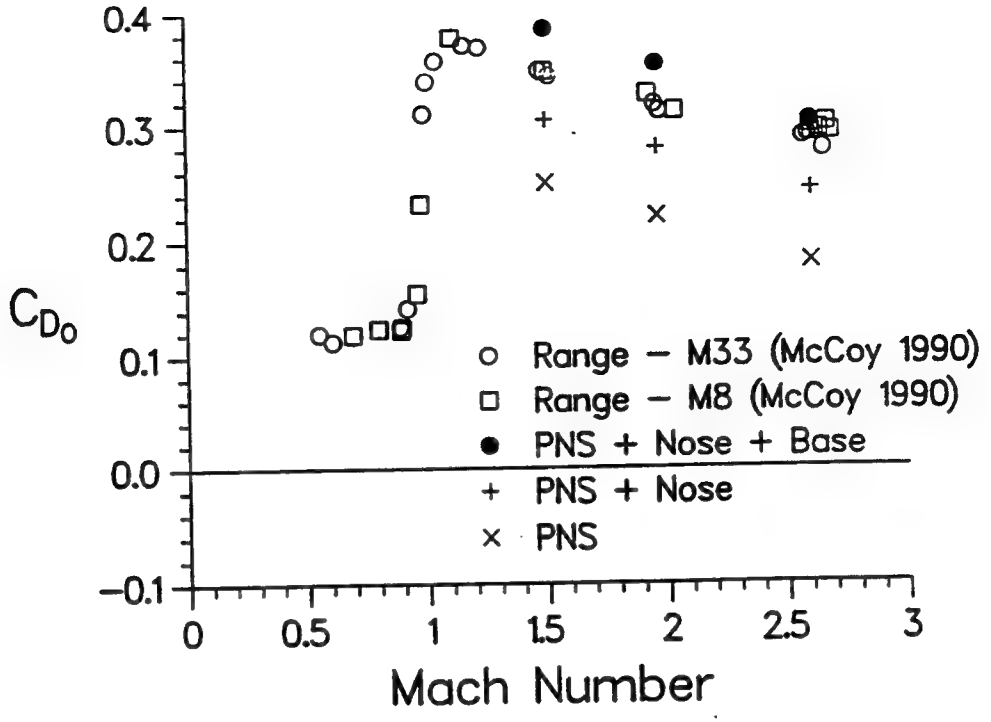

Figure 13. Computed and Measured Zero-Yaw Drag Coefficient Versus Mach Number, M8 and M33 Projectiles

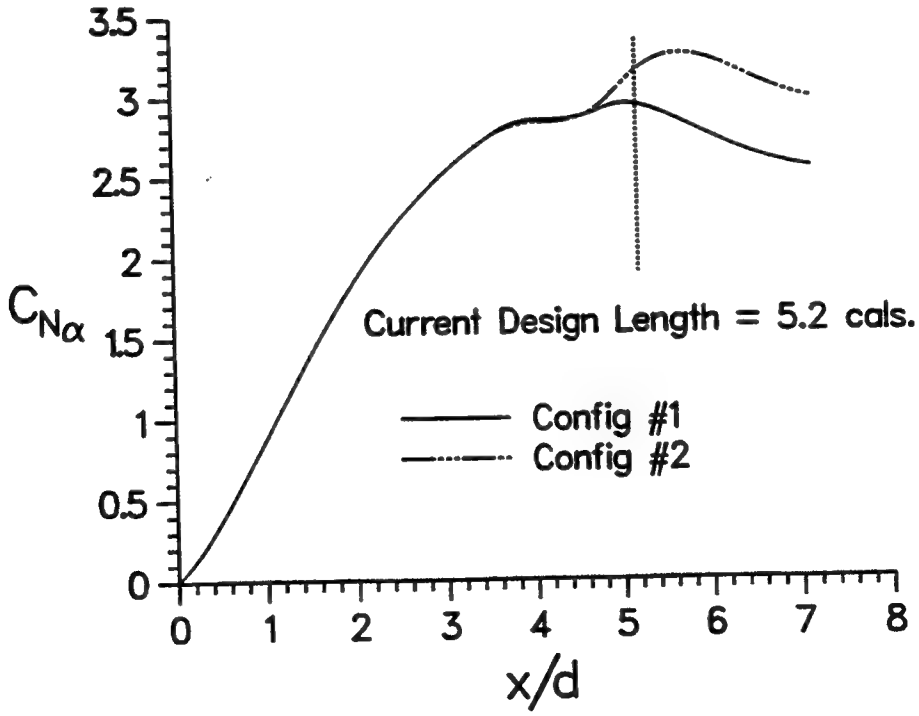

Figure 14. Computed Normal Force Coefficient Versus Body Length, LRTA Configurations, Mach 2.6

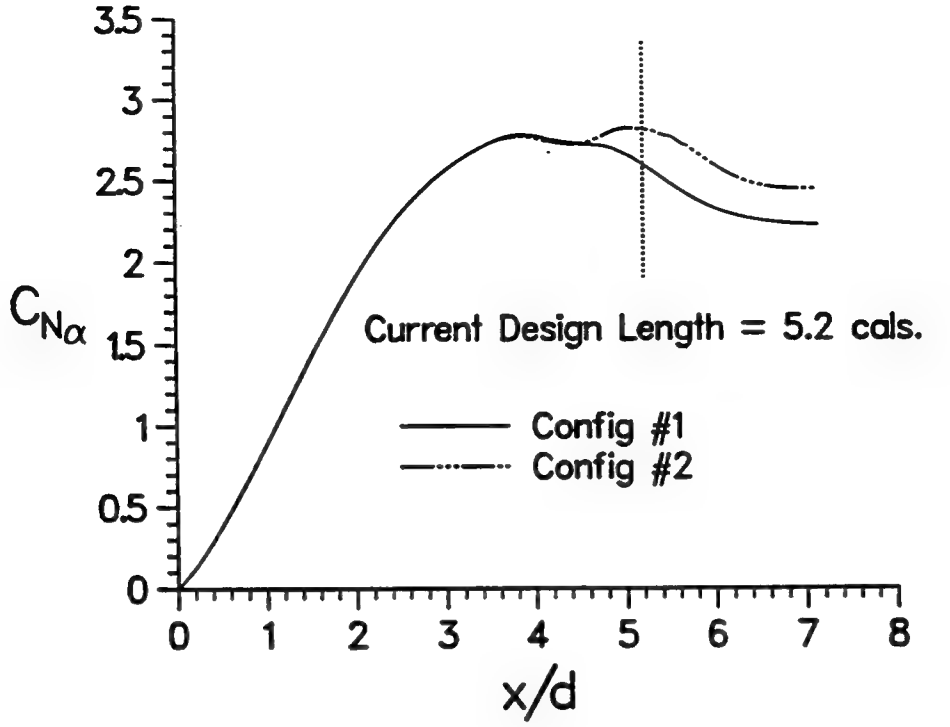

Figure 15. Computed Normal Force Coefficient Versus Body Length, LRTA Configurations, Mach 1.96

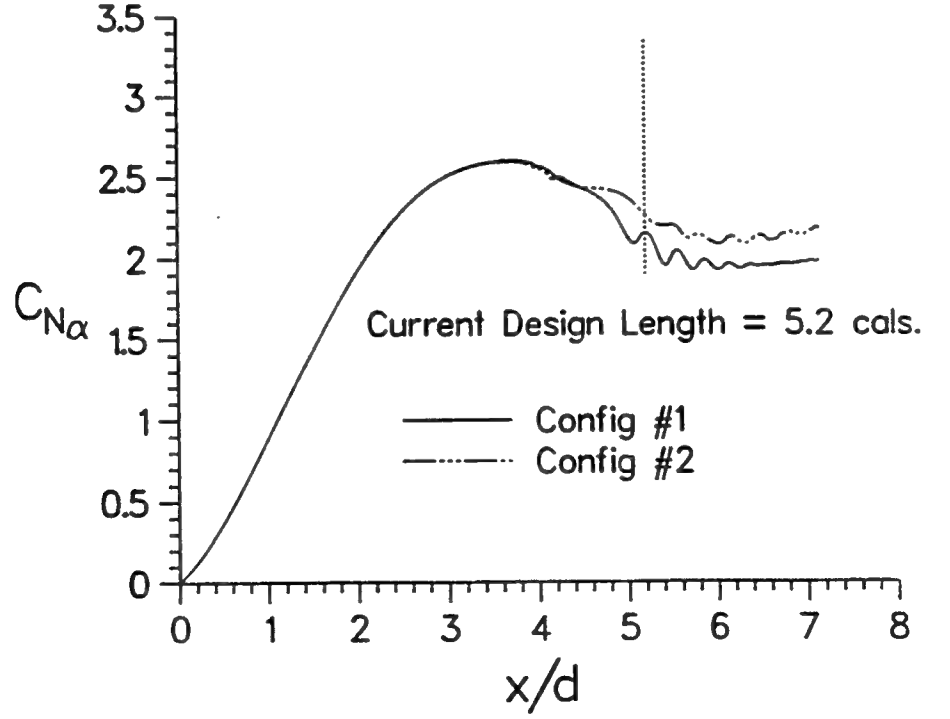

Figure 16. Computed Normal Force Coefficient Versus Body Length, LRTA Configurations, Mach 1.5

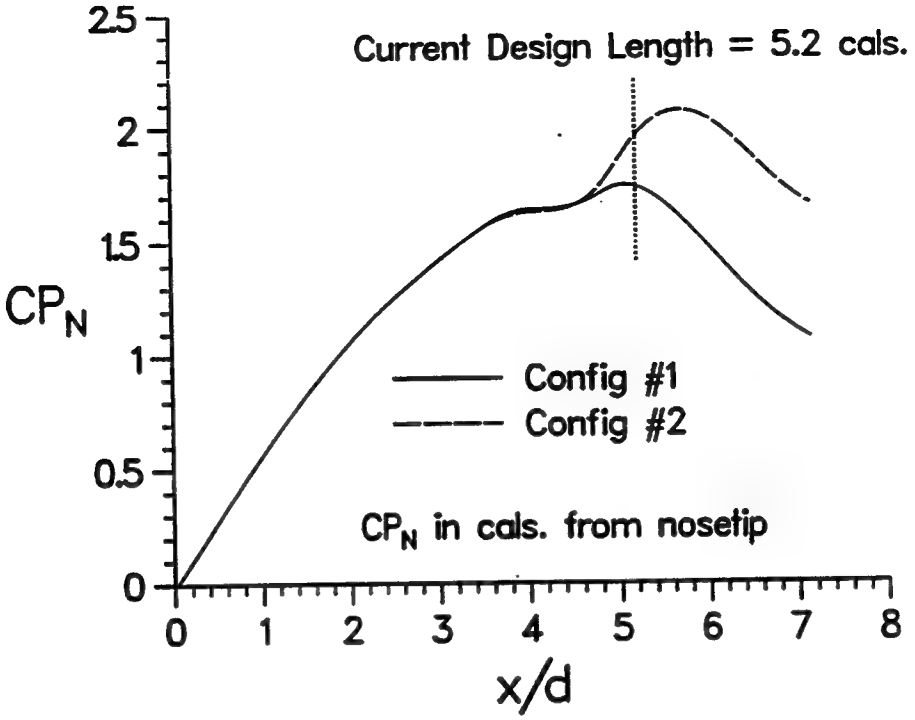

Figure 17. Computed Normal Force Center of Pressure Versus Body Length, LRTA Configurations, Mach 2.6

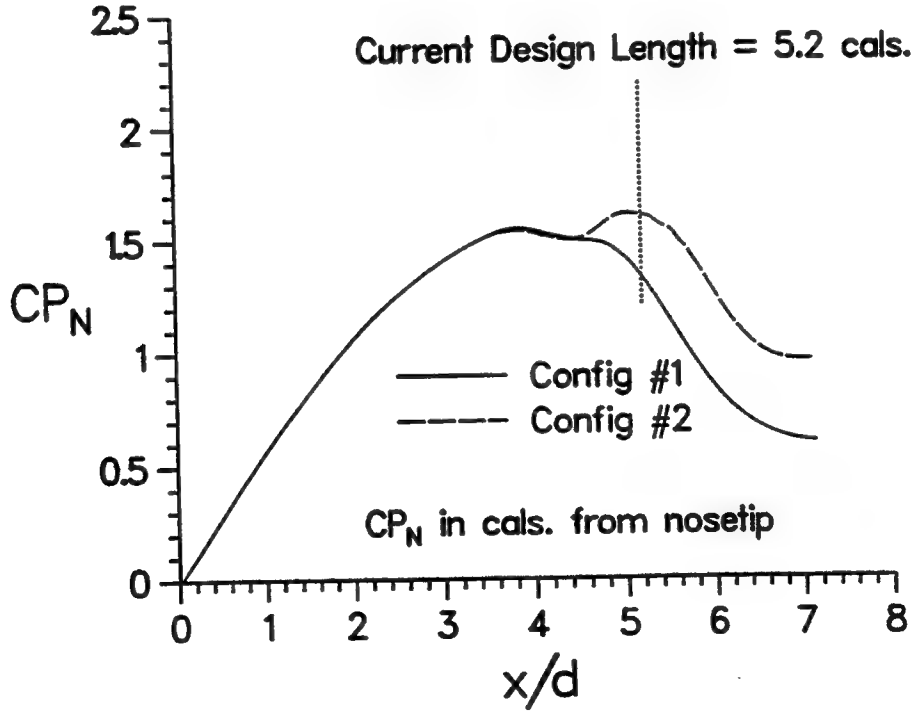

Figure 18. Computed Normal Force Center of Pressure Versus Body Length, LRTA Configurations, Mach 1.96

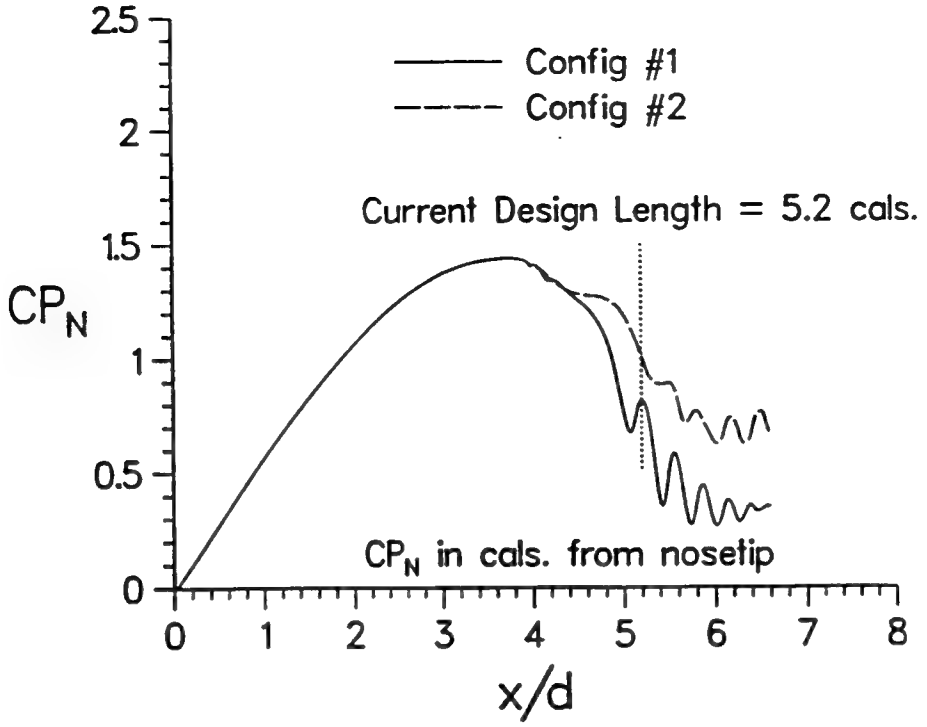

Figure 19. Computed Normal Force Center of Pressure Versus Body Length, LRTA Configurations, Mach 1.5

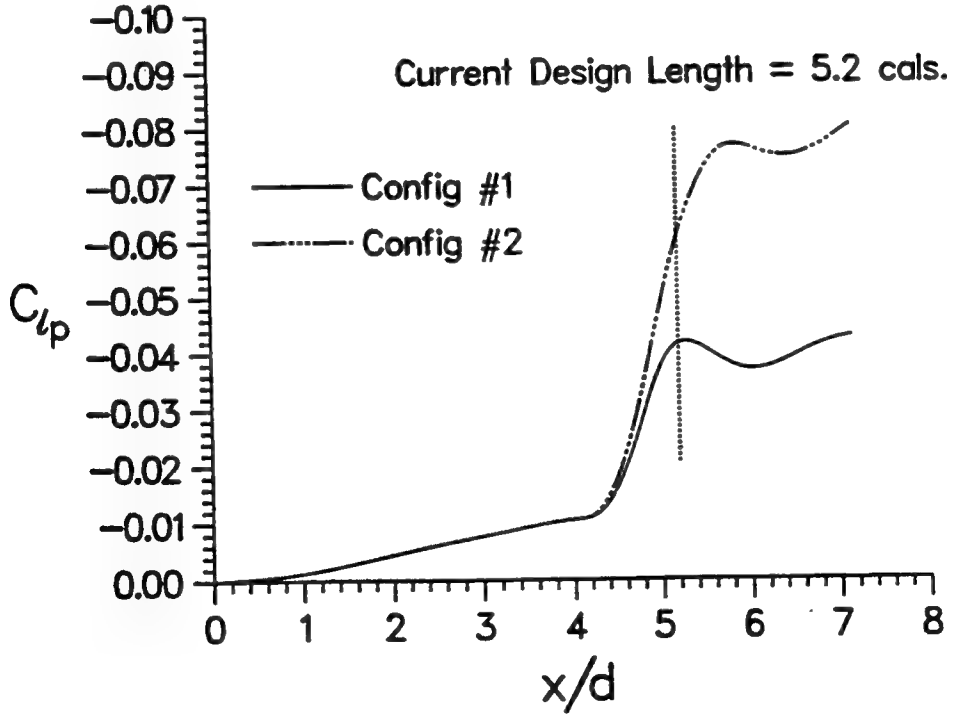

Figure 20. Computed Roll Damping Coefficient Versus Body Length, LRTA Configurations, Mach 2.6

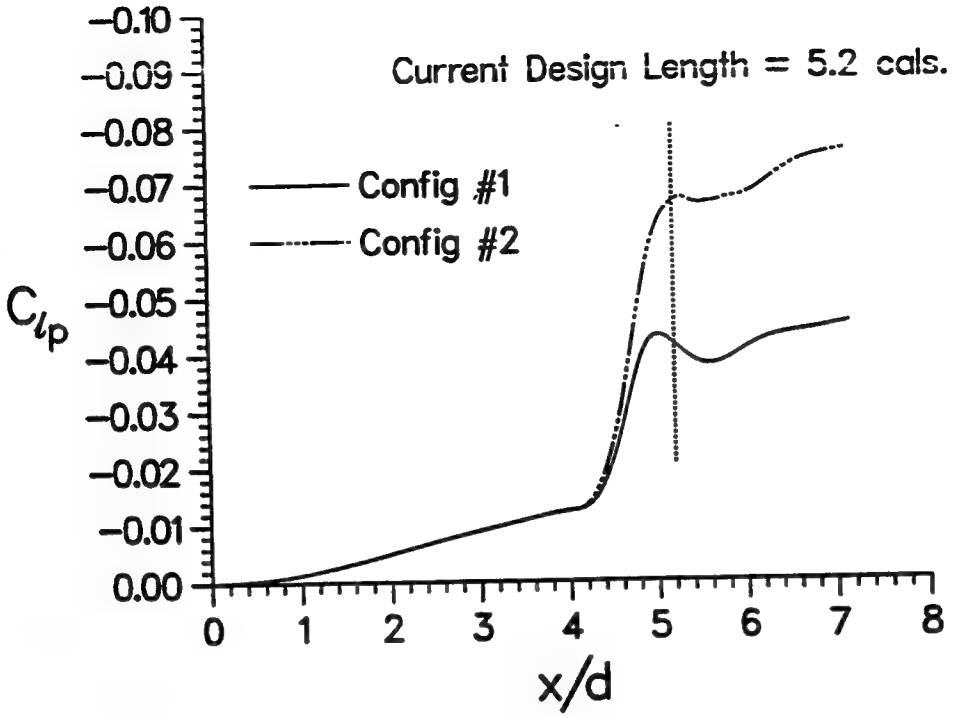

Figure 21. Computed Roll Damping Coefficient Versus Body Length, LRTA Configurations, Mach 1.96

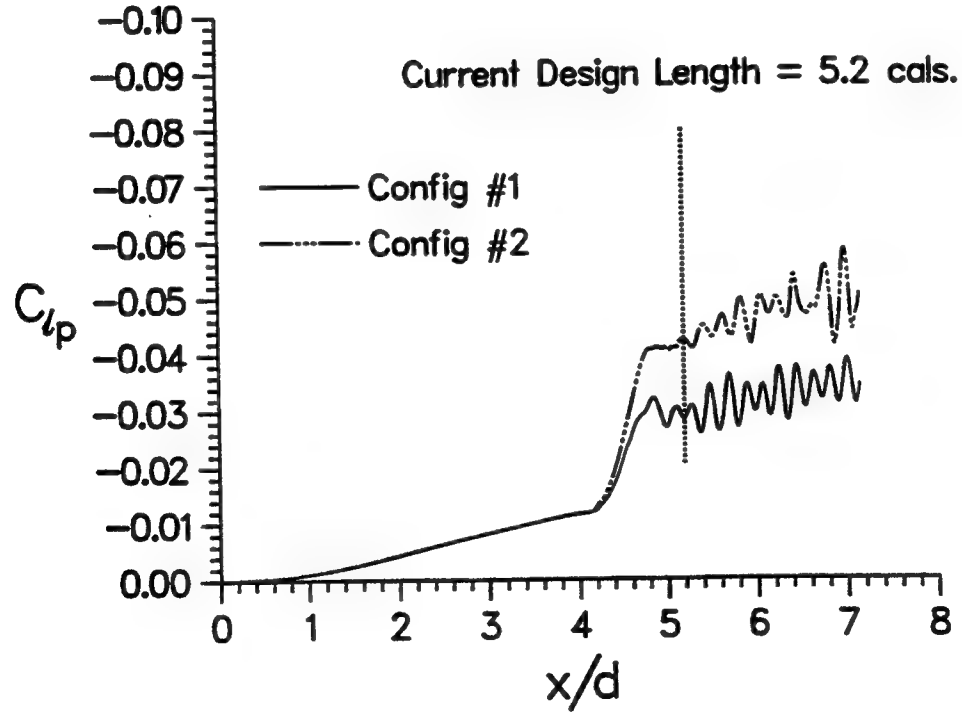

Figure 22. Computed Roll Damping Coefficient Versus Body Length, LRTA Configurations, Mach 1.5

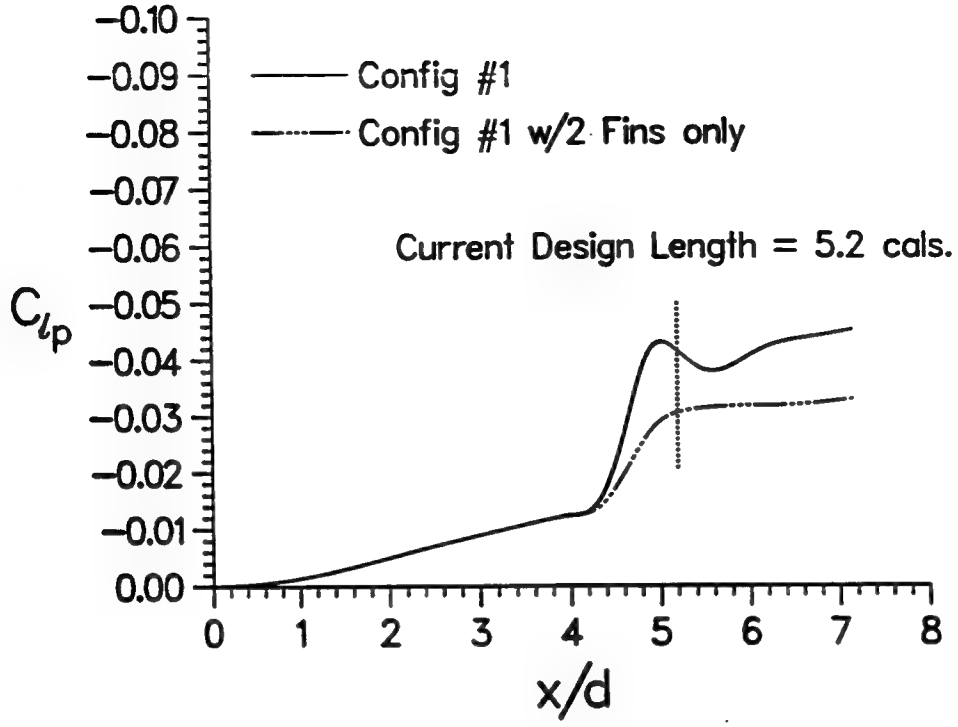

Figure 23. Computed Roll Damping Coefficient for 2-Fin and 4-Fin Configurations Versus Body Length, Mach=1.96

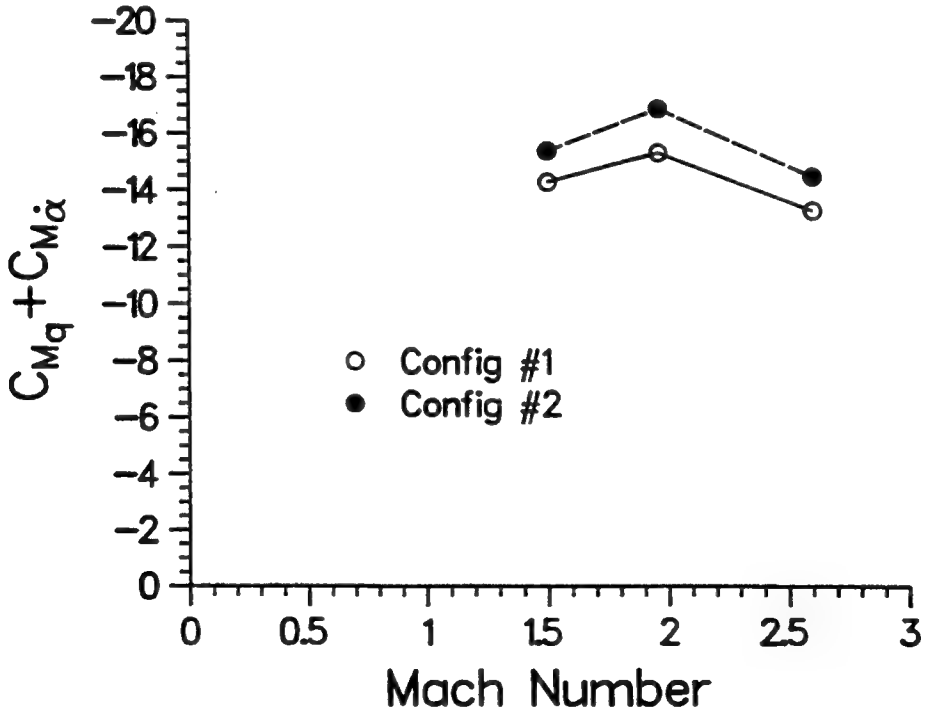

Figure 24. Computed Pitch Damping Moment Coefficient Versus Mach Number, LRTA Configurations

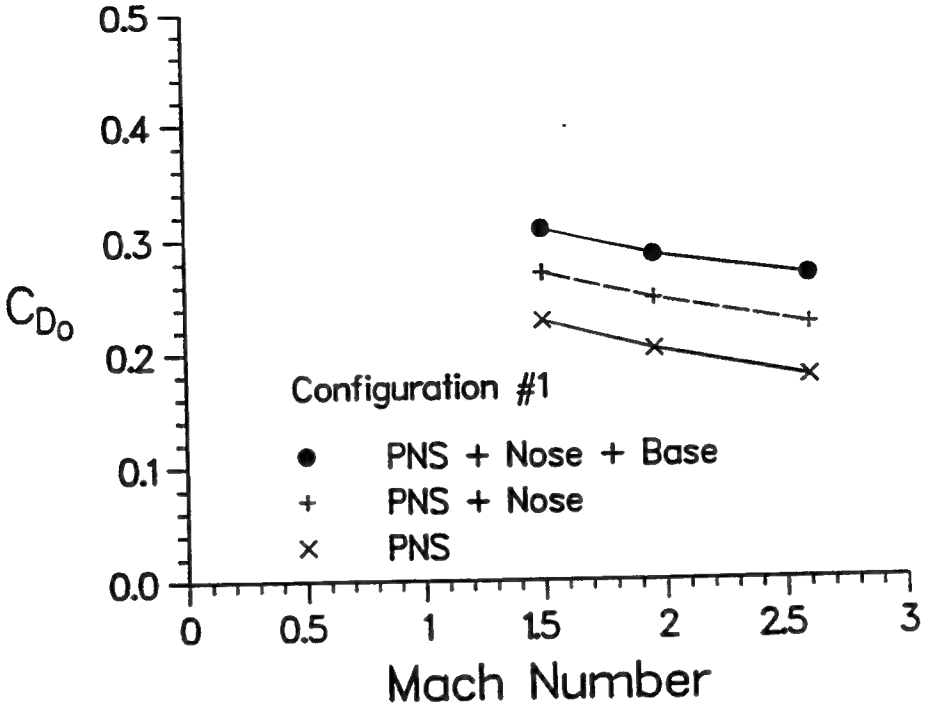

Figure 25. Computed Zero-Yaw Drag Coefficient Versus Mach Number, LRTA Configuration #1

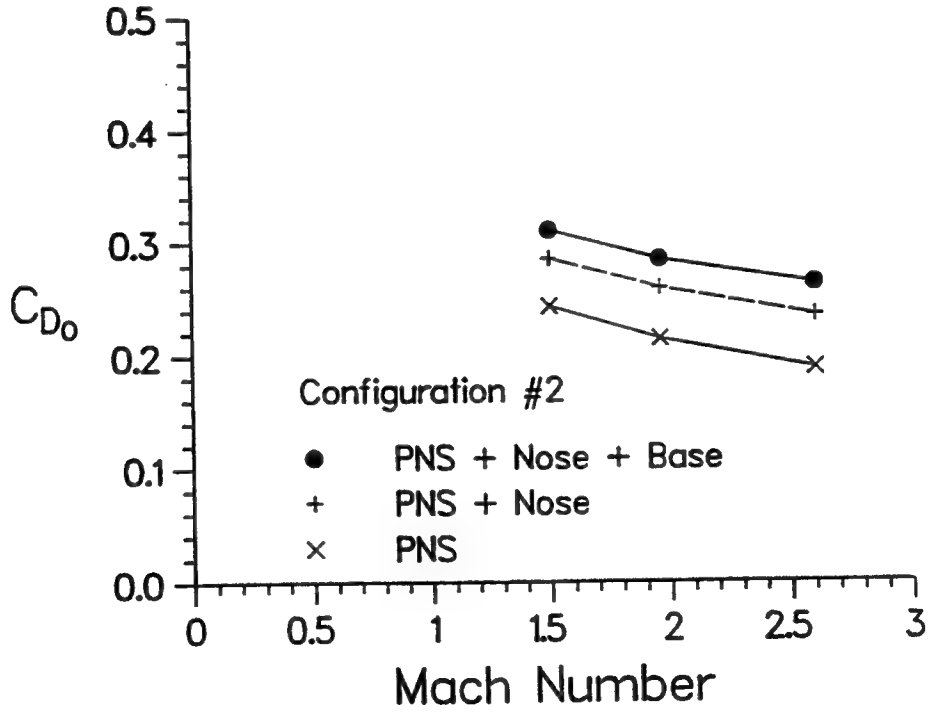

Figure 26. Computed Zero-Yaw Drag Coefficient Versus Mach Number, LRTA Configuration #2

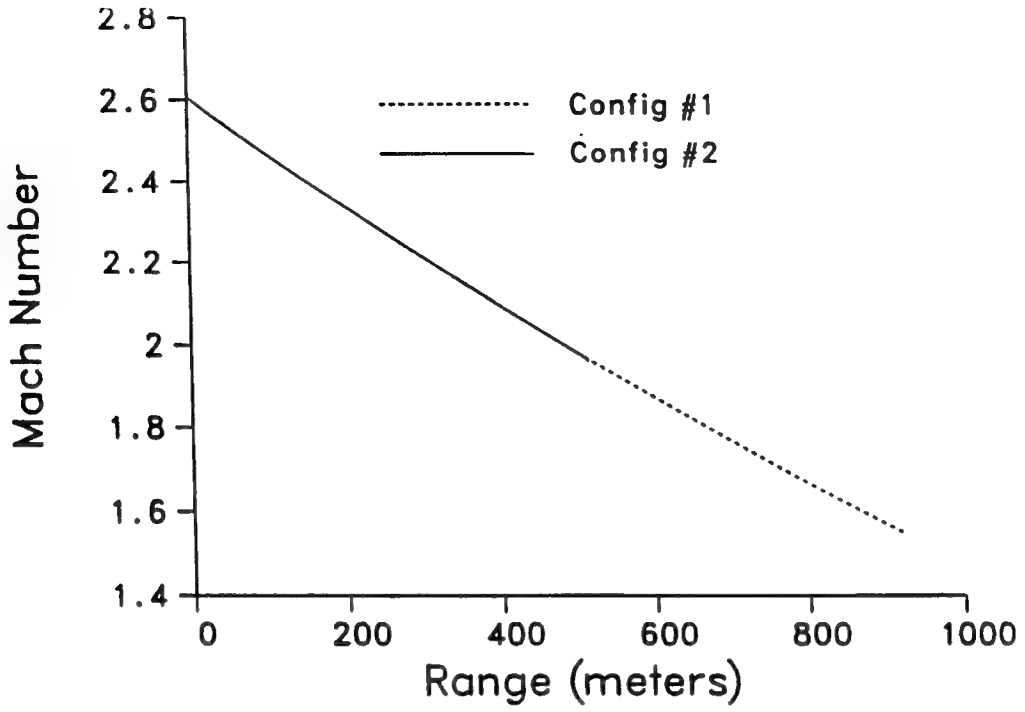

Figure 27. Computed In-Flight Mach Number Versus Range, LRTA Configurations

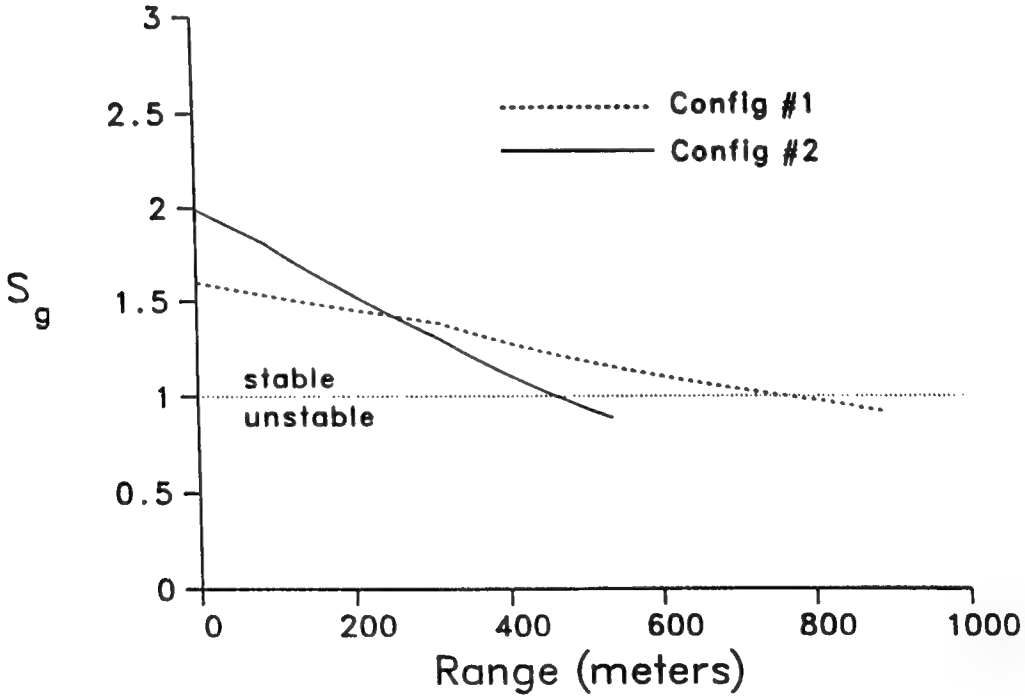

Figure 28. Computed In-Flight Gyroscopic Stability Factor Versus Range, LRTA Configurations

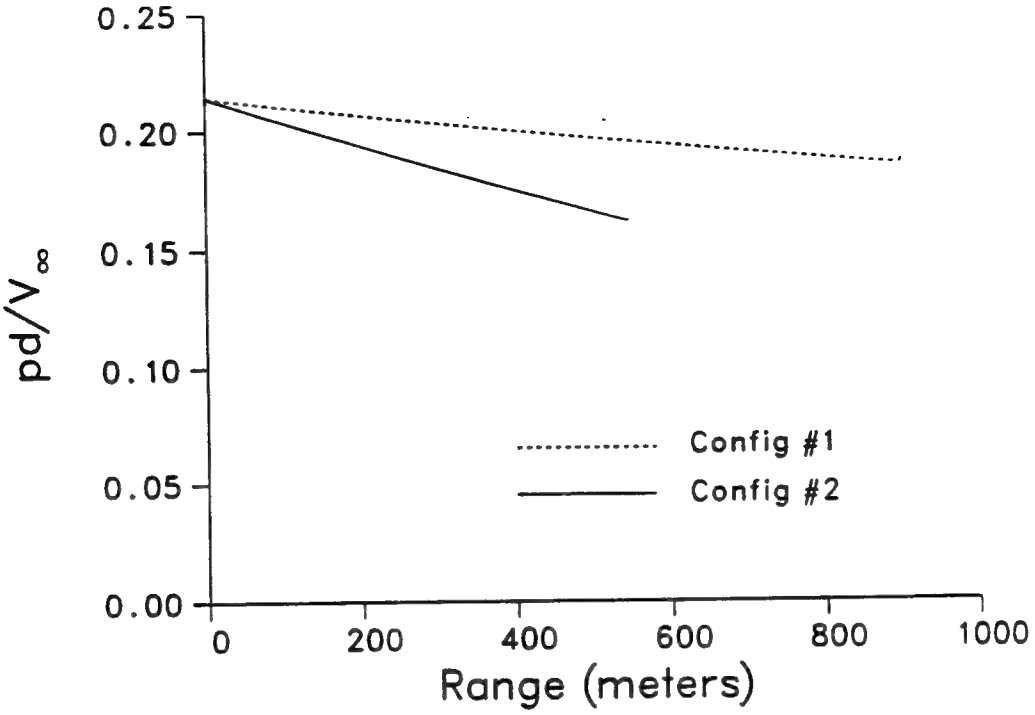

Figure 29. Computed In-Flight Nondimensional Spin Rate Versus Range, LRTA Configurations

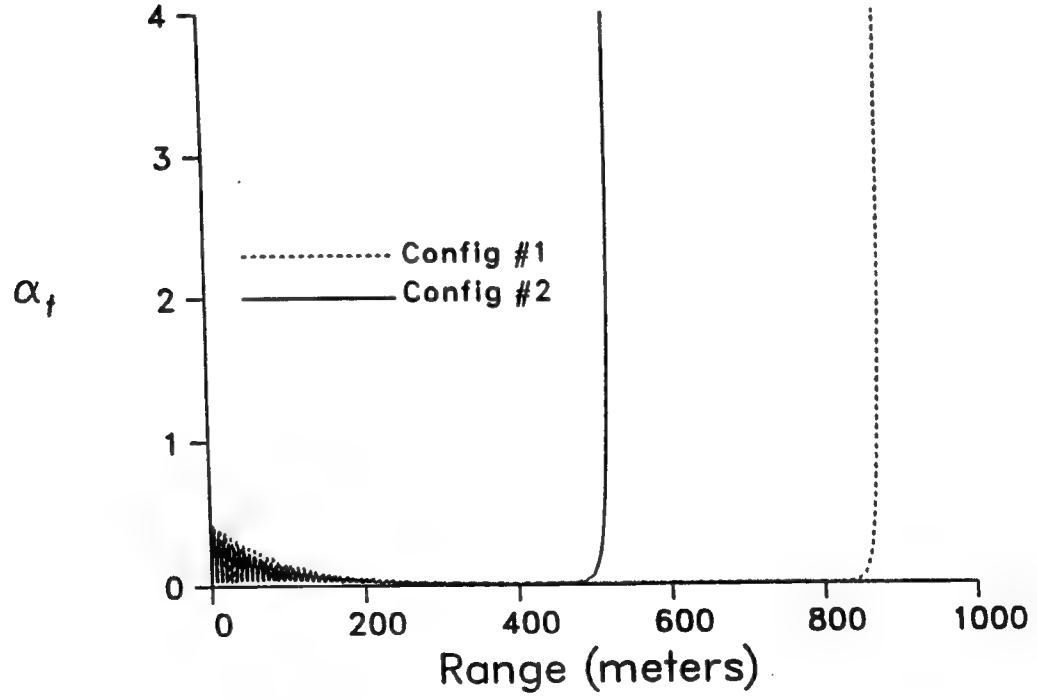

Figure 30. Computed In-Flight Total Angle of Attack Versus Range, LRTA Configurations

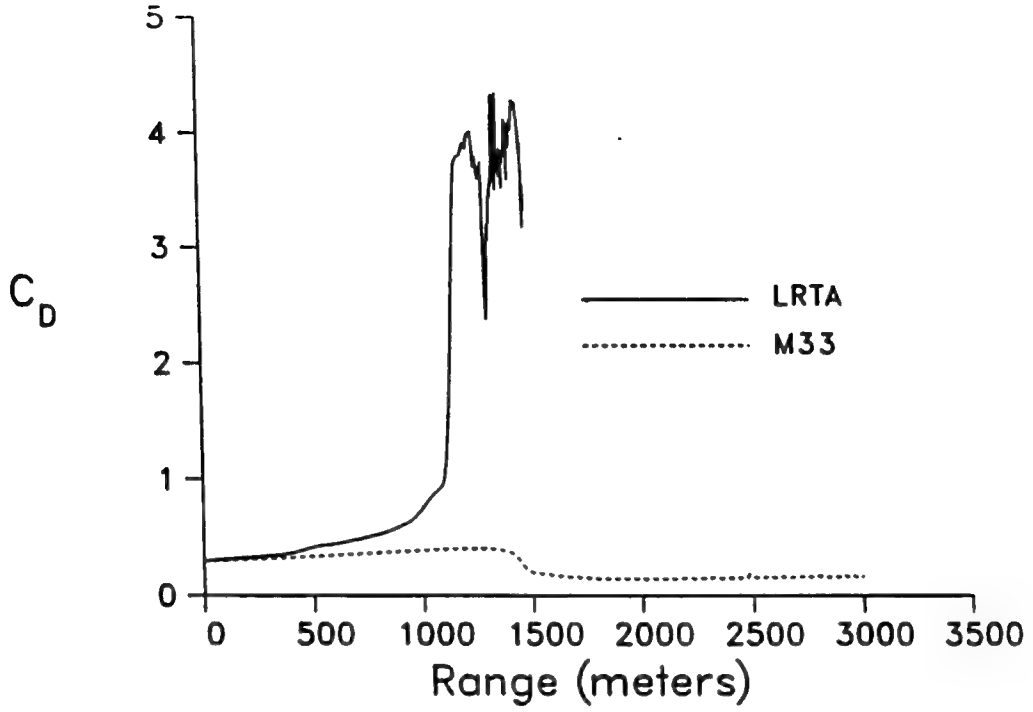

Figure 31. Doppler Radar Measurement of In-Flight Total Drag Versus Range, M33 and LRTA Projectiles

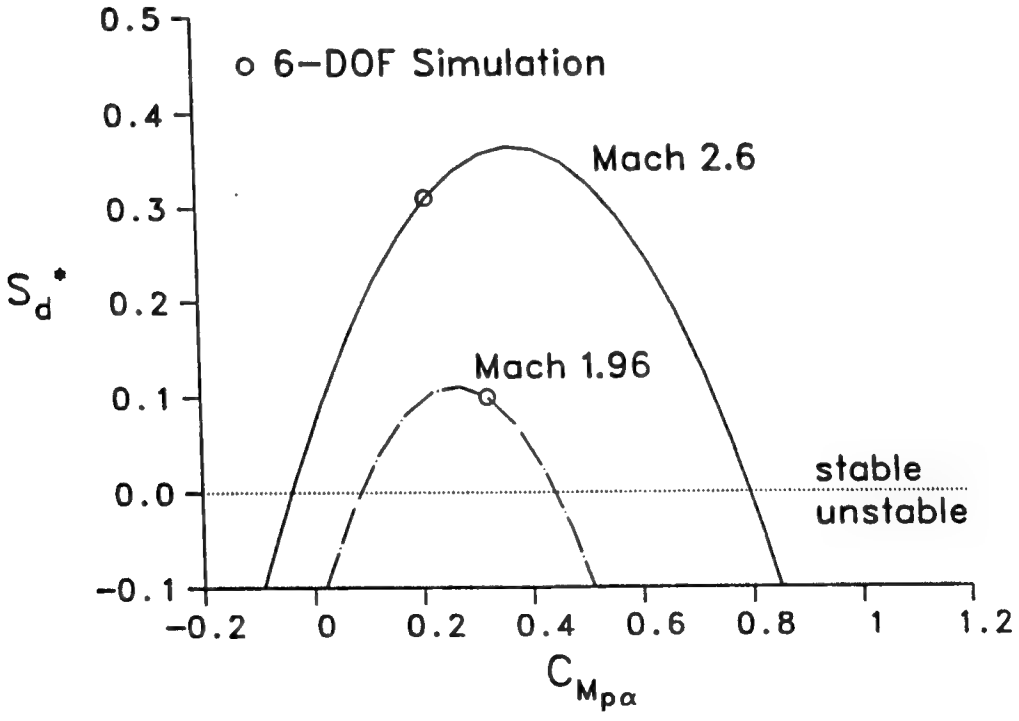

Figure 32. Computed Effect of Magnus Moment Coefficient on Dynamic Stability, LRTA Configuration

6. REFERENCES

Anderson, J.D. Jr."Modern Compressible Flow," 2nd Edition, McGraw-Hill, New York, 1990.

Baldwin, B.S., and H. Lomax. "Thin-Layer Approximation and Algebraic Model for Separated Turbulent Flows," AIAA Paper No. 78-0257, January 1978.

Beam, R., and R.F. Warming. "An Implicit Factored Scheme for the Compressible Navier-Stokes Equations," AIAA Journal, Vol. 16, No. 4, pp. 393-402, 1978.

Fiorellini, A.J., and J. Grau, "An Upgraded Version of the Six-Degree-of-Freedom Trajectory Simulation Computer Program TRAJ," U.S. Army Armament Research, Development, & Engineering Center, Picatinny Arsenal, New Jersey, ASB-IR-08-92, December 1992.

Guidos, B.J., and W.B. Sturek. "Computational Aerodynamic Analysis for a Range-Limited 25mm Training Round," U.S. Army Ballistic Research Laboratory, Aberdeen Proving Ground, Maryland, BRL-TR-2833, August 1987. (AD A185270)

McCoy, R.L. " 'McDrag' - A Computer Program for Estimating the Drag Coefficients of Projectiles," U.S. Army Ballistic Research Laboratory, Aberdeen Proving Ground, Maryland, ARBRL-TR-02293, February 1981. (AD A09810)

McCoy, R.L., "The Aerodynamic Characteristics of .50 Ball, M33, API, M8, and APIT, M20 Ammunition," U.S. Army Ballistic Research Laboratory, Aberdeen Proving Ground, Maryland, BRL-MR-3810, January 1990. (AD A219106)

Murphy, C.H. "Free Flight Motion of Symmetric Missiles," U.S. Army Ballistic Research Laboratories, Aberdeen Proving Ground, Maryland, BRL Report No. 1216, July 1963. (AD A442757)

Platou, A.S. "The Magnus Force on a Finned Body," U.S. Army Ballistic Research Laboratories, Aberdeen Proving Ground, Maryland, BRL Report No. 1193, March 1963. (AD 403767)

Platou, A.S. "An Improved Projectile Boattail," U.S. Army Ballistic Research Laboratory, Aberdeen Proving Ground, Maryland, BRL-MR-2395, July 1974. (AD 785520)

Platou, A.S. "An Improved Projectile Boattail, Part II," U.S. Army Ballistic Research Laboratory, Aberdeen Proving Ground, Maryland, BRL-MR-1866, July 1976. (AD 823839)

Rai, M.M., D.S. Chaussee, and Y.M. Rizk. "Calculation of Viscous Supersonic Flows Over Finned Bodies," AIAA Paper No. 83-1667, July 1983.

Rai, M.M., and D.S. Chaussee. "New Implicit Boundary Procedures: Theory and Applications," AIAA Paper No. 83-0123, January 1983.

Schiff, L.B., and J.L. Steger. "Numerical Simulation of Steady Supersonic Flow," AIAA Paper No. 79-0130, January 1979.

Schiff, L.B., and W.B. Sturek. "Numerical Simulation of Steady Supersonic Flow over an Ogive Cylinder Boattail Body," U.S. Army Ballistic Research Laboratory, Aberdeen Proving Ground, Maryland, ARBRL-TR-02363, September 1981. (AD 106060)

Sturek, W.B., and L.B. Schiff. "Computations of the Magnus Effect for Slender Bodies in Supersonic Flow," U.S. Army Ballistic Research Laboratory, Aberdeen Proving Ground, Maryland, ARBRL-TR-02384, December 1981. (AD 110016)

Weinacht, P., B.J. Guidos, L.D. Kayser, and W.B. Sturek. "PNS Computations for Spinning and Fin-Stabilized Projectiles at Supersonic Speeds," U.S. Army Ballistic Research Laboratory, Aberdeen Proving Ground, Maryland, ARBRL-MR-3464, September 1985. (AD A160393)

Weinacht, P., B.J. Guidos, W.B. Sturek, and B.A. Hodes. "PNS Computations for Spinning Shell at Moderate Angles of Attack and for Long L/D Finned Projectiles," U.S. Army Ballistic Research Laboratory, Aberdeen Proving Ground, Maryland, BRL-MR-3522, June 1986. (AD 169531)

Weinacht, P., and W.B. Sturek. "Computation of the Roll Characteristics of Finned Projectiles," BRL-TR-2931, U.S. Army Ballistic Research Laboratory, Aberdeen Proving Ground, Maryland, June 1988. (AD 197875)

Weinacht, P., and W.B. Sturek. "Navier-Stokes Predictions of Pitch Damping for Finned Projectiles using Steady coning Motion," AIAA Paper 90-3088, August 1990.

Weinacht, P., W. Sturek, and L. Schiff. "Navier-Stokes Predictions of Pitch Damping for Axisymmetric Shell using Steady Coning Motion," AIAA Paper 91-2855, August 1991.

LIST OF SYMBOLS

A	reference area of projectile, evaluated as $\pi d^2/4$
C_D	total drag coefficient
C_{D_0}	zero-yaw drag coefficient
CG	center of gravity, in calibers, measured along x-axis
C_L	lift coefficient
C_{L_α}	lift coefficient, evaluated as C_L/α, α in radians
C_l	roll moment coefficient
C_{l_p}	roll damping coefficient, evaluated as $C_l/(pd/V_\infty)$
C_{M_α}	pitching moment coefficient, evaluated as C_m/α
$C_{M_{p\alpha}}$	Magnus moment coefficient, evaluated as $C_n/(pd/V_\infty)/\alpha$
$C_{M_q} + C_{M_{\dot\alpha}}$	pitch damping moment coefficient
C_m	pitching moment coefficient
C_N	normal force coefficient
C_{N_α}	normal force coefficient, evaluated as C_N/α
$C_{N_{p\alpha}}$	Magnus force coefficient, evaluated as $C_S/(pd/V_\infty)\alpha$
C_n	Magnus moment coefficient
CP_N	normal force center of pressure, in calibers, measured along x-axis
CP_M	Magnus force center of pressure
C_S	Magnus force coefficient
d	reference diameter of projectile
F	aerodynamic force
$\hat{E}, \hat{F}, \hat{G}$	inviscid flux vectors of transformed gas dynamic equations
$\hat{H}_c$	inviscid source term for cylindrical coordinate formulation of transformed gas dynamic equations
I_{xx}	radial moment of inertia
I_{yy}	transverse moment of inertia
l	reference length
M	aerodynamic moment
p	pressure
p	projectile spin rate (rad/s)
q	dynamic pressure, ρv^2
$\bar{Q}$	vector of dependent variables of gas dynamic equations
r	distance from x-axis
$\hat{S}$	viscosity vector of transformed gas dynamic equations

$\hat{S}_c$	viscous source term for cylindrical coordinate formulation of transformed gas dynamic equations
S_d	dynamic stability factor
S_d^*	stability coefficient
S_g	gyroscopic stability factor
V	velocity
u, v, w	velocity components in x, y, z directions
x, y, z	physical Cartesian coordinates

Greek Symbols

α	total angle of attack; pitch angle; yaw angle
ϵ	total energy per unit volume of fluid
ρ	density
ξ, η, ζ	transformed coordinates

Subscript

∞	free stream condition
B	projectile base condition

Note:
Aerodynamic force coefficients are defined as $\frac{F}{\frac{1}{2}q_\infty A}$
Aerodynamic moment coefficients are defined as $\frac{M}{\frac{1}{2}q_\infty Ad}$

NO. OF COPIES	ORGANIZATION
2	ADMINISTRATOR DTIC ATTN DTIC DDA CAMERON STATION ALEXANDRIA VA 22304-6145
1	CDR USAMC ATTN AMCAM 5001 EISENHOWER AVE ALEXANDRIA VA 22333-0001
1	DIR USARL ATTN AMSRL OP SD TA 2800 POWDER MILL RD ADELPHI MD 20783-1145
3	DIR USARL ATTN AMSRL OP SD TL 2800 POWDER MILL RD ADELPHI MD 20783-1145
1	DIR USARL ATTN AMSRL OP SD TP 2800 POWDER MILL RD ADELPHI MD 20783-1145
2	CDR US ARMY ARDEC ATTN SMCAR TDC PCTNY ARSNL NJ 07806-5000
1	DIR BENET LABS ATTN SMCAR CCB TL WATERVLIET NY 12189-4050
1	DIR USA ADVANCED SYSTEMS R&A OFC ATTN AMSAT R NR MS 219 1 AMES RESEARCH CENTER MOFFETT FLD CA 94035-1000
1	CDR US ARMY MICOM ATTN AMSMI RD CS R DOC RDSTN ARSNL AL 35898-5010
1	CDR US ARMY TACOM ATTN AMSTA JSK ARMOR ENG BR WARREN MI 48397-5000

NO. OF COPIES	ORGANIZATION
1	DIR USA TRADOC ANALYSIS CMD ATTN ATRC WSR WSMR NM 88002-5502
1	CMDT US ARMY INFANTRY SCHOOL ATTN ATSH CD SECURITY MGR FT BENNING GA 31905-5660
	ABERDEEN PROVING GROUND
2	DIR USAMSAA ATTN AMXSY D AMXSY MP H COHEN
1	CDR USATECOM ATTN AMSTE TC
1	DIR USAERDEC ATTN SCBRD RT
1	CDR USACBDCOM ATTN AMSCB CII
1	DIR USARL ATTN AMSRL SL I
5	DIR USARL ATTN AMSRL OP AP L

DISTRIBUTION LIST

No. of Copies	Organization
11	Commander US Army Armament RD&E Center ATTN: SMCAR-AET-A, S. Kahn C. Ng M. Amoruso H. Hudgins J. Grau E. Brown B. Wong W. Toledo S. Chung C. Livecchia G. Malejko Picatinny Arsenal, NJ 07806-5000
3	Commander US Army Armament RD&E Center ATTN: SMCAR-CCH-V, B. Konrad E. Fennell T. Louzeiro Picatinny Arsenal, NJ 07806-5000
4	Commander US Army Armament RD&E Center ATTN: SMCAR-FSE, A. Graf D. Ladd E. Andricopoulis K. Cheung Picatinny Arsenal, NJ 07806-5000
6	Commander US Army Armament RD&E Center ATTN: SMCAR-CCL-D, F. Puzycki D. Conway D. Davis K. Hayes M. Pincay W. Schupp Picatinny Arsenal, NJ 07806-5000
1	Commander US Army Missile Command ATTN: AMSMI-RD-SS-AT, B. Walker Redstone Arsenal, AL 35898-5010
3	U.S. Army Research Office ATTN: G. Anderson K. Clark T. Doligowski P.O. Box 12211 Research Triangle Park, NC 27709-2211
2	Director US Army ERDEC ATTN: SCBRD-RTB, D. Weber F. Wrede Aberdeen Proving Ground, MD 21010-5423
2	Director US Army Research Laboratory ATTN: AMSRL-MA-CA, M.R. Fletcher M.E. O'Day 405 Arsenal St. Watertown, MA 02172-0001
2	US Army Benet Laboratory ATTN: SMCAR-CCB-R, S. Sopok P. Aalto Watervaliet, NY 12189
2	United States Military Academy Department of Civil and Mechanical Engineering ATTN: M. Costello A. Dull West Point, NY 10996
7	Director National Aeronautics and Space Administration Ames Research Center ATTN: MS-258-1, L. Schiff T. Holst D. Chaussee T. Edwards G. Molvik S. Lawrence M. Rai Moffett Field, CA 94035

DISTRIBUTION LIST

No. of Copies	Organization
2	Director National Aeronautics and Space Administration Langley Research Center ATTN: Technical Library J. South Langley Station Hampton, VA 23665
3	Air Force Armament Laboratory ATTN: AFATL/FXA, B. Simpson G. Abate R. Adelgren Eglin AFB, FL 32542-5434
2	Commander US Naval Surface Warfare Center Applied Mathematics Branch ATTN: Code R44, A. Wardlaw Code R44, F. Priolo White Oak Laboratory Silver Spring, MD 20903-5000
1	Commander US Naval Surface Weapons Center ATTN: F. Moore Dahlgren, VA 22448
2	USAF Wright Aeronautical Laboratories ATTN: AFWAL/FIMG, J. Shang WPAFB, OH 45433-6553
1	Arnold Engineering & Development Center Calspan Field Service ATTN: MS 600, J. Benek AAFS, TN 37389
2	Director Sandia National Laboratories ATTN: W. Oberkampf W. Wolfe Division 1636 Albuquerque, NM 87185
1	Los Alamos National Laboratory ATTN: MS G770, W. Hogan Los Alamos, NM 87545
1	HQDA ATTN: SARD-TT, F. Milton Washington D.C. 20310-0103
3	Institute for Advanced Technology University of Texas at Austin ATTN: W. Reinecke T. Kiehne D. Barnett 4030-2 W. Braker Lane Austin, TX 78759-5329
2	University of California, Davis Department of Mechanical Engineering ATTN: H. Dwyer B. Meakin Davis, CA 95616
1	University of Maryland Department of Aerospace Engr. ATTN: J. Anderson Jr. College Park, MD 20742
1	University of Texas Department of Aerospace Engineering and Engineering Mechanics ATTN: D. Dolling Austin, Texas 78712-1055
2	University of Delaware Department of Mechanical Engineering ATTN: J. Danberg L. Schwartz Newark, DE 19716
1	University of Cincinnati Department of Aerospace Engineering ATTN: S. Rubin Mail Location 70 Cincinnati, OH 45221

DISTRIBUTION LIST

No. of Copies	Organization
1	University of Florida Department of Engineering Sciences College of Engineering ATTN: C. Hsu Gainesville, FL 32611
1	MDA Engineering, Inc. ATTN: J. Steinbrenner 500 E. Border St., Suite 401 Arlington, TX 76010
2	Alliant Techsystems, Inc. ATTN: M. Swenson R. Burretta Mail Station MN48-3700 7225 Northland Dr. Brooklyn Park, MN 55428
1	General Research Corp. ATTN: H. King P.O. Box 6770 Santa Barbara, CA 93160-6770
5	Kaman Sciences Corp. ATTN: J. Forkois T. Hayden W. Leonard R. Prozan E. Statton 1500 Garden of the Gods Rd. Colorado Springs, CO 80907

USER EVALUATION SHEET/CHANGE OF ADDRESS

This Laboratory undertakes a continuing effort to improve the quality of the reports it publishes. Your comments/answers to the items/questions below will aid us in our efforts.

1. ARL Report Number ARL-TR-662 Date of Report December 1994

2. Date Report Received _____

3. Does this report satisfy a need? (Comment on purpose, related project, or other area of interest for which the report will be used.) _____

4. Specifically, how is the report being used? (Information source, design data, procedure, source of ideas, etc.) _____

5. Has the information in this report led to any quantitative savings as far as man-hours or dollars saved, operating costs avoided, or efficiencies achieved, etc? If so, please elaborate. _____

6. General Comments. What do you think should be changed to improve future reports? (Indicate changes to organization, technical content, format, etc.) _____

CURRENT ADDRESS

_____
Organization

_____
Name

_____
Street or P.O. Box No.

_____
City, State, Zip Code

7. If indicating a Change of Address or Address Correction, please provide the Current or Correct address above and the Old or Incorrect address below.

OLD ADDRESS

_____
Organization

_____
Name

_____
Street or P.O. Box No.

_____
City, State, Zip Code

(Remove this sheet, fold as indicated, tape closed, and mail.)
(DO NOT STAPLE)

DEPARTMENT OF THE ARMY

OFFICIAL BUSINESS

NO POSTAGE
NECESSARY
IF MAILED
IN THE
UNITED STATES

BUSINESS REPLY MAIL
FIRST CLASS PERMIT NO 0001, APG, MD

Postage will be paid by addressee

Director
U.S. Army Research Laboratory
ATTN: AMSRL-OP-AP-L
Aberdeen Proving Ground, MD 21005-5066